NAIST-IS-DD0861208

Doctoral Dissertation

An RF Signal Processing Based Diversity Scheme for MIMO-OFDM Systems

I Gede Puja Astawa

February 15, 2012

Department of Information Systems
Graduate School of Information Science
Nara Institute of Science and Technology

A Doctoral Dissertation
submitted to Graduate School of Information Science,
Nara Institute of Science and Technology
in partial fulfillment of the requirements for the degree of
DOCTOR of ENGINEERING

I Gede Puja Astawa

Thesis Committee:

Professor Minoru Okada	(Supervisor)
Professor Hiroyuki Seki	(Co-supervisor)
Professor Kenji Sugimoto	(Co-supervisor)

An RF Signal Processing Based Diversity Scheme for MIMO-OFDM Systems*

I Gede Puja Astawa

Abstract

Multiple-input and multiple-output (MIMO) is a key technique to achieve broadband wireless communication systems in a limitted frequency bandwidth environment. Orthogonal Frequency Division Multiplexing (OFDM) is an another key technique to establish a reliable wireless transmission over time-dispersive environment. The latest broadband wireless communication systems such as LTE (Long Term Evolution) based Cellular system, W-LAN (Wireless Local Area Network) standard, IEEE 802.11n, and metropolitan area network standard, IEEE 802.16, also known as WiMAX, employ both MIMO and OFDM technologies.

Although MIMO and OFDM are mandatory techniques for broadband wireless communication systems, it has a drawback in hardware size. MIMO transmitter and receiver require the same number of RF front-end circuits. It is difficult to reduce the size and the power consumption of an analog RF front-end circuits, while those from the digital signal processing part can be drastically reduced, thanks to the recent improvement of LSI (Large Scale Integrated circuit) technology. Our research aim is to reduce RF front-end circuit and improve the performance.

The contribution of this dissertation is to improve the bit error rate performance of the MIMO-OFDM system by making efficient use of RF signal processing. Although a 2×2 MIMO-OFDM system can double the capacity without expanding the occupied frequency bandwidth, it does not give additional diversity gain in case of using linear MIMO decomposition algorithm. On the other hand, the proposed RF signal processing assisted by MIMO-OFDM is capable of improving the bit error rate performance.

*Doctoral Dissertation, Department of Information Systems, Graduate School of Information Science, Nara Institute of Science and Technology, NAIST-IS-DD0861208, February 15, 2012.

Computer simulation results show that the proposed scheme gives additional diversity gain. In comparison to the conventional SISO-OFDM, the proposed scheme gives 10.9dB of diversity gain in case of ideal channel estimation, and 9.45 dB when the MMSE (Minimum Mean Square Estimation) - based channel estimator is used.

In order to reduce the computational cost for MIMO decomposition block of the proposed receiver, a new MIMO decoder using Kalman filter with error correction coding (ECC) technique is proposed here. The proposed Kalman filter based MIMO detector still outperforms the conventional coded 2×2 MIMO-OFDM with MLD detector.

Keywords:

MIMO-OFDM systems, RF signal processing, MIMO decomposition, V-BLAST detection, cyclic shift, pilot sequence.

Thank you to the grace of Ida Hyang Widhi Wasa (God Almighty), this dissertation can be completed in a timely manner.

Achievements and Publications

Journal

- I Gede Puja Astawa, M. Okada,"An RF Signal Processing Based Diversity Scheme for MIMO-OFDM Systems," IEICE Trans. on Fundamentals, Vol.E95-A, No.2, pp.515-524, Feb. 2012.

International Conference

- I Gede Puja Astawa, M. Okada,"ESPAR Antenna Based Diversity Scheme for MIMO-OFDM Systems," The International Conference on Embedded Systems and Intelligent Technology (ICESIT) Chiangmai, Thailand, pp.172-175, January 2010.

Contents

List of Figures

List of Tables

Chapter 1

Introduction

MIMO (Multiple Input Multiple Output) is an efficient technology in achieving broadband wireless communication systems in a limited frequency bandwidth environment [1]. Most of the wireless communication systems developed before the mid 1990s is referred to as single input single output (SISO). The systems use single antenna for both transmitter and receiver. Similarly, space diversity scheme having multiple antennas at the receiver is called single input multiple output (SIMO). Space diversity, or SIMO, can improve the bit error rate performance in a multipath fading environment.

MIMO systems offer a significant capacity improvement over SISO system by exploiting multiple antennas at both transmitter and receiver. MIMO not only can improve the bit error rate performance, but also can increase the bit rate without expanding the occupied frequency bandwidth. To develop the broadband mobile wireless communication systems, frequency efficient and reliable digital transmission is very important. MIMO satisfies both requirements.

Although MIMO is thus an atractive technique for broadband wireless communication systems, there are several problems. Some of them are more relevant to equipment vendors or to network carriers, for example, how additional antennas interact with existing base-stations without changing a new air interface, and how to minimize the interference generated by introducing additional antennas. From the operators point of view, however, the most important issue lies on the capacity and spectrum efficiency, that is, how one can best exploit the properties of MIMO links in mobile networks to

improve the spectrum efficiency in bit/s/Hz, the coverage in cell radius, and the quality of service regarding link budget and system capacity. The latest broadband communication systems are LTE (Long Term Evolution) cellular systems, IEEE 802.11n WLAN (Wireless Local Area Network) standard, and IEEE802.16 MAN (Metropolitan Area Network) standard also known as WiMax [1], [2], [3], [4].

In terms of implementing MIMO onto miniature handheld devices, the hardware size and power consumption could be a problem. Generally speaking, the hardware size and power consumption are strictly limitted in handheld devices. However, MIMO requires the same number of Radio Frequency (RF) front-end circuits as the number of antennas. It is generally difficult to reduce the size and the power consumption of an analog RF front-end circuits, while those from the digital signal processing part can be drastically reduced, thanks to the recent improvement in the LSI (Large Scale Integrated circuit) technology. The objective of this research is to reduce the number of RF front-end circuits without sacrificing the performance.

A single RF MIMO system based on RF signal processing has been proposed in [5]. In this work reported in [5], transmitter for MIMO wireless communication uses a single RF front-end at the mobile terminal. Although their proposal can reduce the number of RF front-end, it could not be applied to MIMO-OFDM system. Furthermore, the bit error rate performance in [5] for MIMO system 2×2 using 3 and 5 elements RF signal processing is still worse than MIMO system.

Our research group has proposed a new diversity scheme based on RF signal processing [6]. In this work, the schemes are based on RF signal processing, whose beam direction is oscillated in the symbol time of the received OFDM signal. This scheme gives diversity gain in frequency selective fading channels, but the system presented in [6] is still SISO (Single-Input Single-Output) system.

In this dissertation, I propose an RF signal processing based diversity scheme for 2×2 MIMO-OFDM system using V-BLAST as a MIMO decomposition. Although the proposed scheme is capable of reducing the number of RF front-end circuit, the computational cost in the digital signal processing part was too huge to be implemented. The size of channel matrix to be solved is the same as the number of effective subcarriers. In case of IEEE 802.11n, the matrix size is 56×56. It would be difficult to implement the proposed MIMO receiver as it is with the full-size matrix operations

even if the latest LSI accomodates huge computational cost. Therefore in order to solve this problem, I propose a modification of MIMO decomposition algorithm using a reduced size channel matrix. In the proposed reduced MIMO decomposition algorithm, the channel matrix is divided into two or four sub matrices and each sub-matrix is processed by two or four decomposition processors.

Though the proposed MIMO decomposition algorithm using sub-matrix can reduce the computational cost, but it is still huge and cannot be implemented in some applications where the hardware size is limitted. Then in order to reduce the computational cost, I show another proposal to reduce complexity of computational cost by using Kalman filter based MIMO decomposition and by adding the Error Correction Coding (ECC) technique which is to improve error rate performance.

Computer simulation is carried out in order to confirm the validity of the proposed scheme. The proposed method to simplify the MIMO decomposition algorithm, however, leads the degradation in the bit error rate performance. This thesis reveals the trade-offs among the computational cost and degradation in terms of bit error rate performance through the computer simulation analysis.

1.1. Outline of Dissertation

The rest of the thesis is organized as follows:

- Chapter 2 introduces the overview of MIMO system. In MIMO system I discuss MIMO system model, MIMO detection and also MIMO capacity.

- Chapter 3 shows the overview of MIMO-OFDM systems. Firstly, this chapter gives the principle of OFDM. Then, combination of MIMO and OFDM is discussed.

- Chapter 4 presents an RF signal processing based diversity receiver for the SISO-OFDM system [6]. This chapter describes a new diversity schemes based on RF signal processing. The beam directivity is controlled by the OFDM symbol clock.

- Chapter 5 presents the proposed RF signal processing based diversity scheme

for MIMO-OFDM systems. Also, the computational cost reduction of MIMO decomposition algorithm by making use of sub-matrix.

- Chapter 6 presents computer simulation and discussions. Rayleigh Fading channel model, IEEE 80211.n channel model and WINNER channel model are assumed in the simulation analysis.
- Chapter 7 presents another type of low computational cost MIMO decomposition algorithm using Kalman filter. Furthermore, in this chapter, joint use of Kalman filter and the error corection code (ECC) for MIMO decomposition is proposed.
- Finally, Chapter 8 concludes the thesis.

Chapter 2

Introduction of MIMO System

THIS chapter introduces the principle of Multi-Input Multi-Output (MIMO). The overview of MIMO system is introduced, followed by the MIMO decomposition algorithms. Then MIMO channel model is formulated and the capacity of a MIMO system is analyzed.

2.1. MIMO systems

2.1.1 MIMO System Model

A typical example of the MIMO system is shown in Fig. 2.1. In the figure, the number of transmitter and receiver antenna elements are given by N_T and N_R, respectively. The data stream is divided into N_T sub-streams by the serial-to-parallel converter and applied to the digital modulators followed by the transmitter antennas. The transmitted signals propagate through the MIMO channel and received by N_R antennas. The received signals are applied to demodulators to convert signal into equivalent low pass expressions. Then the signals are collected to the detector, where the MIMO decomposition is carried out. The decomposed signals are finally sent from the parallel to serial converter to recover the transmitted signal.

If $N_T = 1$ and $N_R = 1$ the system turns out to be SISO (Single-Input Single-Output) and the corresponding channel is SISO channel. Likewise if $N_T \geq 2$ and $N_R = 1$ the system is called MISO (Multi-Input Single-Output) and the corresponding channel is

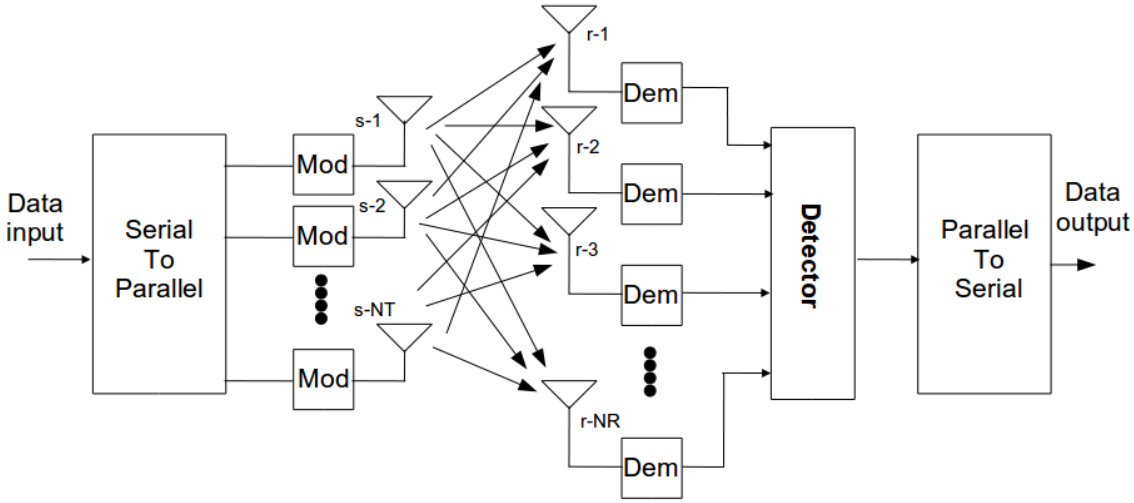

Figure 2.1. A typical MIMO system

MISO channel, and again if $N_T = 1$ and $N_R \geq 2$ the system is SIMO (Single-Input Multi-Output).

The equivalent lowpass expression of channel impulse response between i-th receive antenna from j-th transmit antenna at time t is expressed as $h_{ij}(\tau; t)$, where τ is delay variable. Furthermore, let us assume the channel matrix as:

$$\mathbf{H}(\tau; t) = \begin{pmatrix} h_{11}(\tau; t) & h_{12}(\tau; t) & \cdots & h_{1N_T}(\tau; t) \\ h_{21}(\tau; t) & h_{22}(\tau; t) & \cdots & h_{2N_T}(\tau; t) \\ \vdots & \vdots & \vdots & \\ h_{N_R1}(\tau; t) & h_{N_R2}(\tau; t) & \cdots & h_{N_RN_T}(\tau; t) \end{pmatrix}, \tag{2.1}$$

The signal received at the i-th antenna is given by

$$\begin{aligned} r_i(t) &= \sum_{j=1}^{N_T} \int_{-\infty}^{+\infty} h_{ij}(\tau; t) s_j(t - \tau) \\ &= \sum_{j=1}^{N_T} h_{ij}(\tau; t) * s_j(\tau), \end{aligned} \tag{2.2}$$

where $s_j(t)$ is the signal transmitted from the j-th transmit antenna, $j = 1, 2, \cdots, N_T$, i starts from 1 until N_R, and $*$ denotes convolution. And in matrix form the equation

(2.2) can be expressed as

$$\mathbf{r}(t) = \mathbf{H}(\tau; t) * \mathbf{s}(\tau), \tag{2.3}$$

where $\mathbf{s}(t)$ and $\mathbf{r}(t)$ are N_T and N_R dimensional vectors, respectively that. In the following, a frequency flat channel is assumed. That is, the impulse response can be written as:

$$h_{ij}(\tau; t) = h_{ij}(t)\delta(\tau), \tag{2.4}$$

where $\delta(\tau)$ is the Dirac delta function. The channel matrix can be modified as:

$$\mathbf{H}(t) = \begin{pmatrix} h_{11}(t) & h_{12}(t) & \cdots & h_{1N_T}(t) \\ h_{21}(t) & h_{22}(t) & \cdots & h_{2N_T}(t) \\ \vdots & \vdots & \vdots & \\ h_{N_R1}(t) & h_{N_R2}(t) & \cdots & h_{N_RN_T}(t) \end{pmatrix}, \tag{2.5}$$

The signal received at the i-th antenna is given by

$$r_i(t) = \sum_{j=1}^{N_T} h_{ij}(t)s_j(t), \tag{2.6}$$

where $i = 1, 2, \cdots, N_R$. The equation (2.6) can be expressed in matrix form as:

$$\mathbf{r}(t) = \mathbf{H}(t)\mathbf{s}(t). \tag{2.7}$$

As in equation (2.6), each received signal is the sum of the transmitted signals. In order to recover the transmitted signals, the receiver is required to decompose the received signals. In the following, I will describe several type of MIMO detector.

2.1.2 MIMO Detectors

Zero Forcing

In this section one of equalizer types in MIMO system is described. Figure 2.2 illustrates the block diagram of the equivalent discrete-time domain equalizer. This output equalizer can be expressed by the simple equation $C(z) = \frac{1}{F(z)}$. This equation is known as zero forcing equalizer.

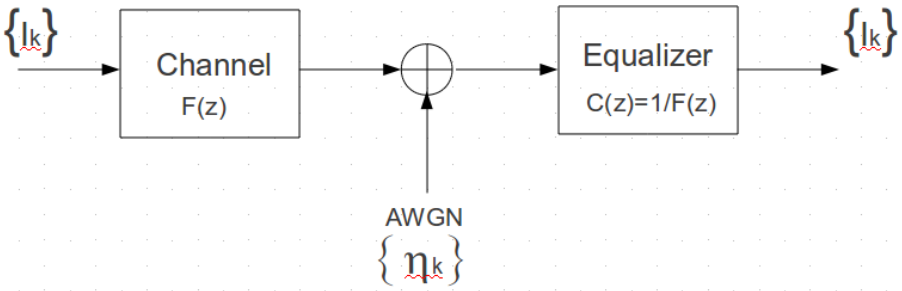

Figure 2.2. Block diagram of MIMO channel with zero forcing equalizer

The zero forcing MIMO detector is derived by the same manner. If the channel transfer matrix $\mathbf{H}$ is invertible, $\mathbf{H}$ is inverted and the transmitted MIMO vector $\mathbf{x}$ is estimated as

$$\hat{\mathbf{x}} = \mathbf{H}^{-1}\mathbf{r}. \tag{2.8}$$

In this technique, each substream in turn is considered to be the desired signal, and the remaining data streams are considered as interferers. Nulling of the interferers is performed by linearly weighting the received signals such that all interfering terms are cancelled. Sometimes if the channel matrix, $\mathbf{H}$ is not square, the inverse matrix $\mathbf{H}$ obtained by the following pseudo-inverse matrix :

$$\mathbf{W} = \mathbf{H}^{\dagger} = \left(\mathbf{H}^{H}\mathbf{H}\right)^{-1}\mathbf{H}. \tag{2.9}$$

Then the transmitted MIMO vector $\mathbf{x}$ can be estimated as shown in Eq.(2.10)

$$\hat{\mathbf{x}}_{\mathbf{ZF}} = \mathbf{W}\mathbf{r} = \mathbf{H}^{\dagger}\mathbf{r} = \left(\mathbf{H}^{H}\mathbf{H}\right)^{-1}\mathbf{H}\mathbf{r} \tag{2.10}$$

Although the zero forcing is a simple algorithm, it suffers from noise enhancement.

Minimum Mean Square Error (MMSE)

Another approach in estimation theory to the problem of estimating a random vector $\mathbf{x}$ on the basis of observations $\mathbf{r}$ is to choose a function $f(r)$ that minimizes the Mean Square Error (MSE). The MMSE equalizer is given by

$$\hat{\mathbf{x}}_{MMSE} = \mathbf{W}\mathbf{r} = \left(\alpha\mathbf{I}_{N_t} + \mathbf{H}^{H}\mathbf{H}\right)^{-1}\mathbf{H}^{H}\mathbf{r}, \tag{2.11}$$

where α denotes the variance of the noise and $\mathbf{I}$ denotes the identity matrix. The advantage of MMSE equalizer against zero forcing equalizer is to reduce the noise enhancement. It is noted that the MMSE in equation (2.11) reaches ZF when $\alpha = 0$.

V-BLAST Detection

The block diagram of V-BLAST system is illustrated in Fig. 2.3. The input data stream is divided into M substreams, and each substream is encoded into symbols and fed to its corresponding transmitter. The M transmitters operate at the same frequency channel at symbol rate $\frac{1}{T}$ symbol/sec.

In the receiver, N receivers receive the signals radiated from all M transmit antennas. If fading channel is flat then the channel matrix transfer function is $\mathbf{H}_{N\times M}$, where h_{ij} is the complex transfer function between the receiver i and transmitter j. In general, the system satisfies $M \leq N$.

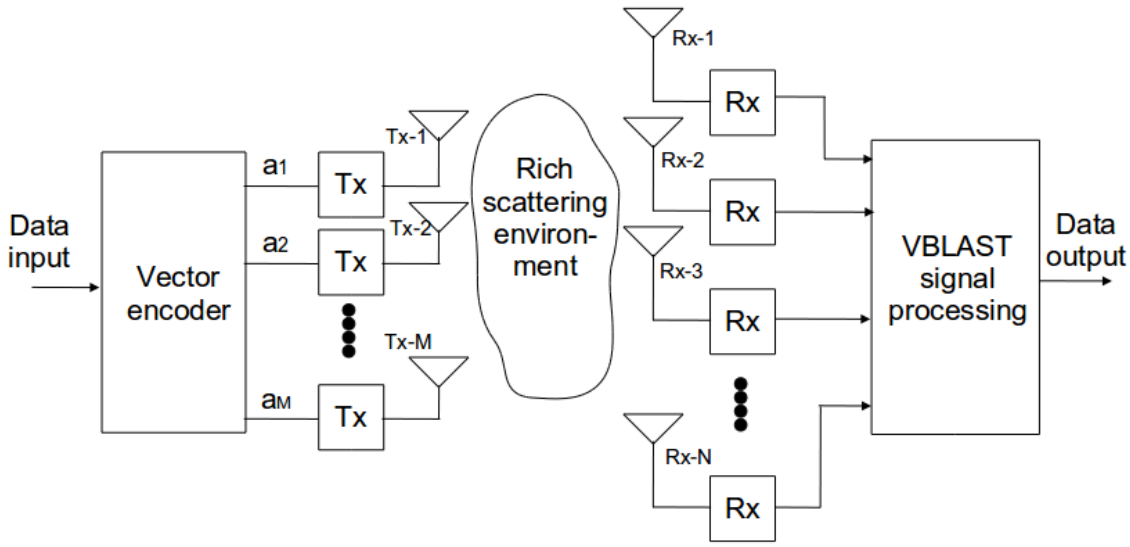

Figure 2.3. Block diagram of V-BLAST system

In the V-BLAST detection algorithms, the symbols are first decomposed using a linear process such as zero-forcing (ZF) or minimum mean square error (MMSE) algorithm. One of the decomposed signals is applied to the modulator to re-generate the tentative estimate of the transmitted signal, and the re-generated signal is subtracted from the received signals in order to reduce the interfering signal components. This

process is repeated until all N symbols are decomposed [7]. The decomposition process of V-BLAST algorithm is given by,

- Ordering : choose the best channel
- Nulling : use Zero Forcing (ZF) or MMSE
- Slicing : make a symbol decision
- Canceling : subtract the detected symbol
- Iteration : going to the first step to detect the next symbol.

Now let us go into the detail of the V-BLAST algorithm. Let $\mathbf{a} = [a_1, a_2, \cdots, a_{N_t}]^T$ be the transmit symbol vector, then the received symbol is $\mathbf{r} = \mathbf{Ha} + \mathbf{v}$ where $\mathbf{H}$ is the channel matrix. Let us also assume that $\mathbf{S} = \{k_1, k_2, \cdots, k_{N_t}\}$ denotes the set of substream data index to be decomposed. As an initialization, I set $\mathbf{H}_1 = \mathbf{H}$, $\mathbf{r} = \mathbf{r}_1$ and i = 1.

The decomposition procedure of the V-BLAST is as follows:

- **INITIALIZATION**
- $i \leftarrow 1$
- compute $\mathbb{G} = \mathbf{H}_i^{\dagger}$ for ZF and $\mathbf{G} = \mathbf{H}^H \left(\mathbf{HH}^H + \sigma^2 \mathbf{I}\right)^{-1}$ for MMSE
- Ordering, by using $k_1 = \underbrace{\arg\min}_{j} \|(\mathbb{G}_1)_j\|^2$
- **RECURSION**
- Nulling vector, $\mathbf{w}_{ki} = (\mathbb{G}_i)_{ki}$
- Nulling, $\mathbf{y}_{k_i} = \mathbf{w}_{ki} r_i$
- Hard decision, $\hat{\mathbf{a}}_{k_i} = \mathbf{Q}(\mathbf{y}_{k_i})$
- Canceling, $\mathbf{r}_{i+1} = \mathbf{r}_i - \hat{\mathbf{a}}_{k_i} \mathbf{H}_{k_i}$
- $\mathbb{G}_{i+1} = \mathbf{H}^{\dagger}{}_{k_i}$

- $k_{1+1} = \underbrace{\arg\min}_{j \notin \{k_1, k_2, \cdots, k_i\}} \|(\mathbb{G}_{i+1})_j\|^2$
- $i \leftarrow i + 1$

where

- $\mathbf{H}^{\dagger}$ denotes the Moore-Penrose pseudoinverse
- $(\mathbf{H})_{k_i}$ denotes the k_i-th column
- $(\mathbf{H})_{\bar{k}_i}$ denotes the matrix obtained by zeroing columns $k_1, k_2, \cdots, k_i$ of $\mathbf{H}$

In order to make clear the explanation of V-BLAST detection, I give an example of the V-BLAST detection for 3×5 MIMO systems. The channel matrix is given by

$$\mathbf{H} = \begin{pmatrix} h_{11} & h_{12} & h_{13} \\ h_{21} & h_{22} & h_{23} \\ h_{31} & h_{32} & h_{33} \\ h_{41} & h_{42} & h_{43} \\ h_{51} & h_{52} & h_{53} \end{pmatrix}. \tag{2.12}$$

Let $\mathbf{a} = [a_1, a_2, a_3]^T$ be the transmit symbol vector, and the received symbol is $\mathbf{r} = [r_1, r_2, r_3, r_4, r_5]^T$. I will find transmitted symbol which is estimated. Based on V-BLAST detection procedure at the INITIALIZATION stage, $\mathbb{G} = \mathbf{H}^{\dagger}$ is shown as follows:

$$\mathbb{G}_1 = \mathbf{H}^{\dagger} = \begin{pmatrix} h_{ab} & h_{ac} & h_{ad} & h_{ae} & h_{af} \\ h_{ba} & h_{bc} & h_{bd} & h_{be} & h_{bf} \\ h_{ca} & h_{cb} & h_{cd} & h_{ce} & h_{cf} \end{pmatrix}. \tag{2.13}$$

Then we can get the order of the channel using $k_1 = \underbrace{\arg\min}_{j} \|(\mathbb{G}_1)_j\|^2$. It is shown as follows:

$$\mathbb{G}_1 = \left[\begin{array}{ccccc} h_{ab} & h_{ac} & h_{ad} & h_{ae} & h_{af} \\ \hline h_{ba} & h_{bc} & h_{bd} & h_{be} & h_{bf} \\ \hline h_{ca} & h_{cb} & h_{cd} & h_{ce} & h_{cf} \end{array}\right]. \tag{2.14}$$

In order to explain the algorithm, it is assume that the k_1 is 2. At the RECURSION stage, the number of iterations are three. For the first iteration, the nulling vector is

given by

$$\mathbf{w}_2 = (\mathbf{G_1})_2 = \begin{pmatrix} h_{ba} & h_{bc} & h_{bd} & h_{be} & h_{bf} \end{pmatrix}. \tag{2.15}$$

Using the nulling process, we can get the tentative decomposed symbol as

$$\mathbf{y}_2 = \mathbf{w}_2 \mathbf{r}_1 \tag{2.16}$$

$$= \begin{pmatrix} h_{ba} & h_{bc} & h_{bd} & h_{be} & h_{bf} \end{pmatrix} \begin{pmatrix} r_1 \\ r_2 \\ r_3 \\ r_4 \\ r_5 \end{pmatrix}. \tag{2.17}$$

Using hard decision, the second transmitted symbol can be decoded as

$$\hat{a}_2 = \mathbf{Q}(\mathbf{y_2}). \tag{2.18}$$

In the next step, the obtained symbol is subtracted from the received signal in order to reduce the interference. The received signal after cancelling the second symbol is given by

$$\mathbf{r}_2 = \mathbf{r}_1 - \hat{a}_2 (H)_2 \tag{2.19}$$

$$= \begin{pmatrix} r_1 \\ r_2 \\ r_3 \\ r_4 \\ r_5 \end{pmatrix} - \hat{a}_2 \begin{pmatrix} h_{12} \\ h_{22} \\ h_{32} \\ h_{42} \\ h_{52} \end{pmatrix}. \tag{2.20}$$

After cancelling process, let's update $\mathbb{G}$ as

$$\mathbb{G}_2 = \mathbf{H}_{\bar{2}}^{\dagger} \tag{2.21}$$

$$= \begin{pmatrix} h_{13} & h_{23} & h_{33} & h_{43} & h_{53} \\ 0 & 0 & 0 & 0 & 0 \\ h_{11} & h_{21} & h_{31} & h_{41} & h_{51} \end{pmatrix} \tag{2.22}$$

where

$$\mathbf{H}_{\bar{2}} = \begin{pmatrix} h_{11} & 0 & h_{13} \\ h_{21} & 0 & h_{23} \\ h_{31} & 0 & h_{33} \\ h_{41} & 0 & h_{43} \\ h_{51} & 0 & h_{53} \end{pmatrix}. \tag{2.23}$$

On the next step, the same decomposition and canceling process is carried out. The second best channel k is determined using $k_2 = \underbrace{\arg\min}_{j} \|(\mathbb{G}_2)_j\|^2$. $\mathbb{G}_2$ is given by

$$\mathbb{G}_2 = \begin{bmatrix} \overline{\begin{matrix} h_{13} & h_{23} & h_{33} & h_{43} & h_{53} \end{matrix}} \\ 0 \quad 0 \quad 0 \quad 0 \quad 0 \\ h_{11} \quad h_{21} \quad h_{31} \quad h_{41} \quad h_{51} \end{bmatrix}. \tag{2.24}$$

Let's assume k_2 is 1. At the second iteration, nulling vector is given by

$$\mathbf{w}_1 = (\mathbf{G_2})_1 = \begin{pmatrix} h_{13} & h_{23} & h_{33} & h_{43} & h_{53} \end{pmatrix}. \tag{2.25}$$

Using cancelling process, the second decomposed signal is given by

$$\mathbf{y}_1 = \mathbf{w}_1 \mathbf{r}_2 \tag{2.26}$$

$$= \begin{pmatrix} h_{13} & h_{23} & h_{33} & h_{43} & h_{53} \end{pmatrix} \begin{pmatrix} r_1 \\ r_2 \\ r_3 \\ r_4 \\ r_5 \end{pmatrix}. \tag{2.27}$$

Using hard decision again, the first transmission symbol is obtained as

$$\hat{a}_1 = \mathbf{Q}(\mathbf{y_1}) \tag{2.28}$$

Again, the the estimated symbol component is subtracted from the received signal as:

$$\mathbf{r}_3 = \mathbf{r}_2 - \hat{a}_1 (H)_1 \tag{2.29}$$

$$= \begin{pmatrix} r_1 \\ r_2 \\ r_3 \\ r_4 \\ r_5 \end{pmatrix} - \hat{a}_1 \begin{pmatrix} h_{12} \\ h_{22} \\ h_{32} \\ h_{42} \\ h_{52} \end{pmatrix}. \tag{2.30}$$

And after cancelling process, $\mathbb{G}$ is updated to:

$$\mathbb{G}_3 = \mathbf{H}_{\bar{1}}^{\dagger} \tag{2.31}$$

$$= \begin{pmatrix} 0 & 0 & 0 & 0 & 0 \\ 0 & 0 & 0 & 0 & 0 \\ h_{11} & h_{21} & h_{31} & h_{41} & h_{51} \end{pmatrix} \tag{2.32}$$

where

$$\mathbf{H}_{\bar{1}} = \begin{pmatrix} h_{11} & 0 & 0 \\ h_{21} & 0 & 0 \\ h_{31} & 0 & 0 \\ h_{41} & 0 & 0 \\ h_{51} & 0 & 0 \end{pmatrix}. \tag{2.33}$$

At the last step, channel matrix is updated as:

$$\mathbb{G}_3 = \begin{bmatrix} \overline{\begin{matrix} 0 & 0 & 0 & 0 & 0 \end{matrix}} \\ \begin{matrix} 0 & 0 & 0 & 0 & 0 \end{matrix} \\ \begin{matrix} h_{11} & h_{21} & h_{31} & h_{41} & h_{51} \end{matrix} \end{bmatrix}. \tag{2.34}$$

The remaining nulling vector w_3 is again given by

$$\mathbf{w}_3 = (\mathbf{G_3})_3 = \begin{pmatrix} h_{11} & h_{21} & h_{31} & h_{41} & h_{51} \end{pmatrix}. \tag{2.35}$$

And the transmitted symbol can be estimated by:

$$\mathbf{y}_3 = \mathbf{w}_3 \mathbf{r}_3 \tag{2.36}$$

$$= \begin{pmatrix} h_{11} & h_{21} & h_{31} & h_{41} & h_{51} \end{pmatrix} \begin{pmatrix} r_1 \\ r_2 \\ r_3 \\ r_4 \\ r_5 \end{pmatrix}. \tag{2.37}$$

Finally, the remaining third transmitted symbol is demodulated as follows:

$$\hat{a}_3 = \mathbf{Q}(\mathbf{y_3}) \tag{2.38}$$

The output of the V-BLAST processor is as follows:

$$\hat{\mathbf{a}} = \{\hat{a}_1 \ \hat{a}_2 \ \hat{a}_3\}. \tag{2.39}$$

Maximum Likelihood Detection (MLD)

Maximum Likelihood Detection (MLD) is a method that performs a maximum likelihood search over all possible transmitted vectors $\mathbf{x}$. The equation is expressed as

$$\hat{\mathbf{x}}_{MLD} = \arg \underbrace{\min}_{x_j \in \{x_1, \cdots, x_l\}} \|\mathbf{r} - \mathbf{H}\mathbf{x}\|^2 \tag{2.40}$$

where a search is performed over all vectors x_i that is a part of the ensemble $x_1, \cdots, x_l$ formed by all possible transmitted vectors. Their number equals to

$$\text{PROB} = M^{N_t} \tag{2.41}$$

where PROB denotes combination of all possible transmitted vectors, M denotes number of constellation point, and N_t number of transmitter antenna elements. The MLD is the high precession of the equalizer but the disadvantage is the complexity. The computational cost grows exponentially with increase in N_t.

2.1.3 Gain and Properties of MIMO

MIMO has many advantages over traditional SISO such as the beamforming gain, the diversity gain, and the multiplexing gain. The beamforming and diversity gains exist in SIMO and MISO respectively too. The multiplexing gain, however, is a unique characteristic of MIMO channels. Some gains can be simultaneously achieved while others compete and establish a tradeoff. Beamforming gain, or the improvement in SINR (signal to interference-plus-noise power ratio) is obtained by coherently combining the signals on multiple transmit or multiple receive dimensions. If the BER of a communication system is plotted with respect to the transmitted power or the received power per antenna (using a logarithmic scale), the beamforming gain is characterized as a shift of the curve due to the gain in SINR. In diversity gain, or the improvement in link reliability, the received symbol is obtained by receiving replicas of the information signal through independently faded channels. This type of diversity is clearly related to the random nature of the channel and is closely connected to the specific channel statistics. If the BER of a communication system is plotted with respect to the transmitted power or the received power per antenna (using a logarithmic scale), the diversity gain is easily characterized as the increase of the slope of the curve in the low

BER region. Multiplexing gain is equivalent to the increase in bit rate, at no additional power consumption, obtained through multiple dimensions at both sides of the communication link. While the beamforming and the diversity gains can be obtained when multiple dimensions are present at either the transmitter or the receiver side. That is, the multiplexing gain requires multiple dimensions at both ends of the link.

2.2. Capacity of MIMO System

This section briefly introduces the capacity of MIMO system according to the reference [8]. In order to determine the capacity of MIMO system, the mutual information has to be computed between the transmitted signal vector $\mathbf{s}$ and the received vector $\mathbf{r}$, denoted as $I(\mathbf{s};\mathbf{y})$. Then the probability distribution of the signal vector $\mathbf{s}$ is optimized to maximize $I(\mathbf{s};\mathbf{y})$. The channel capacity is given by

$$C = \max_{p(s)} I(\mathbf{s};\mathbf{y}) \tag{2.42}$$

Through some derivations, the capacity of the MIMO channel is given by

$$C = \max_{tr(R_{ss})=\varepsilon_s} \log_2 \det\left(\mathbf{I}_{N_R} + \frac{1}{N_0}\mathbf{H}\mathbf{R}_{ss}\mathbf{H}^H\right) \text{ bps/Hz} \tag{2.43}$$

where ε_s is the energy per symbol, $\mathbf{R}_{ss}$ is the covariance matrix of the transmitted signals and $tr(*)$ is the trace of $*$. In case that the signal among the N_T transmitters are statistically independent, $\mathbf{R}_{ss} = \frac{\varepsilon_s}{N_T} I_{N_T}$ the capacity is rewritten as according to the statistically independent assumption of the transmitted signals

$$C = \log_2 \det\left(\mathbf{I}_{N_R} + \frac{\varepsilon_s}{N_T N_0}\mathbf{H}\mathbf{H}^H\right) \text{ bps/Hz} \tag{2.44}$$

The equation (2.44) can also be modified in terms of eigen value decomposition, $\mathbf{H}\mathbf{H}^H = \mathbf{Q}\Delta\mathbf{Q}^H$, where $\mathbf{Q}$ is the unitary matrix whose columns are the eigen vectors of $\mathbf{H}\mathbf{H}^H$ and Δ are the diagonal matrix whose diagonal elements are the eigen values. Then the equation (2.44) can be rewritten as

$$C = \sum_{i=1}^{r} \log_2\left(1 + \frac{\varepsilon_s}{N_T N_0}\lambda_i\right) \tag{2.45}$$

where r is the rank of the channel matrix $\mathbf{H}$.

In case of SISO, equation (2.45) is reduced to

$$C_{siso} = \log_2\left(1 + \frac{\varepsilon_s}{N_0}|h_{11}|^2\right) \text{bps/Hz} \tag{2.46}$$

where $\lambda_1 = |h_{11}|^2$.

In case of SIMO, by substituting $\lambda_1 = \|\mathbf{h}\|_F^2 = \sum_{i=1}^{N_R} |h_{i1}|^2$ to equation (2.45), the capacity is given by

$$C_{simo} = \log_2\left(1 + \frac{\varepsilon_s}{N_0}\sum_{i=1}^{N_R} |h_{i1}|^2\right) \text{bps/Hz} \tag{2.47}$$

Also in MISO, $\lambda_1 = \|\mathbf{h}\|_F^2 = \sum_{j=1}^{N_T} |h_{1j}|^2$ is applied to the equation (2.45), the capacity is given by

$$C_{miso} = \log_2\left(1 + \frac{\varepsilon_s}{N_T N_0}\sum_{j=1}^{N_T} |h_{1j}|^2\right) \text{bps/Hz} \tag{2.48}$$

Chapter 3

Overview MIMO-OFDM system

THE growing demand of multimedia services and the growth of internet related contents lead to increasing interest to high speed communications. The requirement for wide bandwidth and flexibility impose the use of efficient transmission methods that would fit to the characteristics of wideband channels especially in wireless environment where the channel is very challenging. In wireless environment the signal is propagating from the transmitter to the receiver along a number of different paths, collectively referred as multipath. While propagating the signal power drops due to three effects: path loss, macroscopic fading and microscopic fading. Fading of the signal can be mitigated by different diversity techniques. To obtain diversity, the signal is transmitted through multiple (ideally) independent fading paths e.g. in time, frequency or space and combined constructively at the receiver. Multiple-Input Multiple-Output (MIMO) exploits spatial diversity by having several transmiter and receiver antennas. However MIMO principles assume frequency flat fading MIMO channels. OFDM is a modulation method known for its capability to mitigate multipath. In OFDM the high speed data stream is divided into N_c narrowband data streams, N_c corresponding to the subcarriers or subchannels i.e. one OFDM symbol consists of N symbols modulated for example by QAM or PSK. As a result the symbol duration is N times longer than in a single carrier system with the same symbol rate. The symbol duration is made even longer by adding a cyclic prefix to each symbol. As long as the cyclic prefix is longer than the channel delay spread OFDM offers inter-symbol interference (ISI) free transmission. Another key advantage of OFDM is that it dramatically reduces equalization

complexity by enabling equalization in the frequency domain. OFDM, implemented with IFFT at the transmitter and FFT at the receiver, converts the wideband signal, affected by frequency selective fading, into N narrowband flat fading signals [1] thus the equalization can be performed in the frequency domain by a scalar division carrier-wise with the subcarrier related channel coefficients. The channel should be known or learned at the receiver. The combination MIMO-OFDM is very natural and beneficial since OFDM enables support of more antennas and larger bandwidth since it simplifies equalization dramatically in MIMO systems.

In this chapter, first the principle of OFDM is explained in section 3.1. Then, the combination of MIMO and OFDM is described in section 3.2. Section 3.3 introduces MIMO-OFDM which shows that the MIMO-OFDM processing transfers the wide-band frequency-selective MIMO channel into a number of parallel flat-fading MIMO subchannels. In the next section the frequency-selective MIMO capacity is determined and the corresponding outage PER is defined.

3.1. Introduction of Orthogonal Frequency Division Multiplexing (OFDM) System

Orthogonal Frequency Division Multiplexing (OFDM) is a multi-carrier modulation technique. It achieves high speed data rates, prevents inter-symbol interference (ISI), and overcomes multi-path fading. It also allows communications in areas where non-line-of-sight (NLOS) is a limiting factor for wireless deployments. OFDM modulation divides the available spectrum channel into several or more independent sub-carriers. This is achieved by making all the sub-carriers orthogonal to one another, preventing interference between the closely spaced sub-carriers. In an OFDM signal, all the orthogonal sub-carriers are transmitted simultaneously.

3.1.1 Generation of Subcarriers using the IFFT

An OFDM signal consists of a sum of subcarriers that are modulated by using phase shift keying (PSK) or quadrature amplitudo modulation (QAM). An OFDM symbol is

given by

$$
\begin{aligned}
s(t) &= \Re\left\{\sum_{i=-\frac{N_s}{2}}^{\frac{N_s}{2}-1} d_{i+N_s/2}\exp(j2\pi(f_c - \frac{i+0.5}{T})(t-t_s))\right\}, t_s \le t \le t_s + T \\
s(t) &= 0, t < t_s \wedge t > t_s + T
\end{aligned} \tag{3.1}
$$

where d_i are the complex QAM symbols, N_s is the number of subcarriers, T is the symbol duration, and f_c the carrier frequency and t_s is the guard interval.

The equation (3.1) is often shown as a complex baseband notation :

$$
\begin{aligned}
s_{lp}(t) &= \sum_{i=-\frac{N_s}{2}}^{\frac{N_s}{2}-1} d_{i+N_s/2}\exp(j2\pi(-\frac{i}{T})(t-t_s)), t_s \le t \le t_s + T \\
s_{lp}(t) &= 0, t < t_s \wedge t > t_s + T
\end{aligned} \tag{3.2}
$$

This equation reperesents the real and imaginary parts that correspond to the in-phase and quadrature parts of the OFDM signal, which have to be multiplied by a cosine and sine of the desired carrier frequency to produce the final OFDM signal. The block diagram of OFDM modulator is shown in Fig. 3.1. If the k-th subcarrier from (3.2) is demodulated by downconverting the signal with a frequency of k/T and then integrating the signal over T seconds, the results are as shown in (3.3).

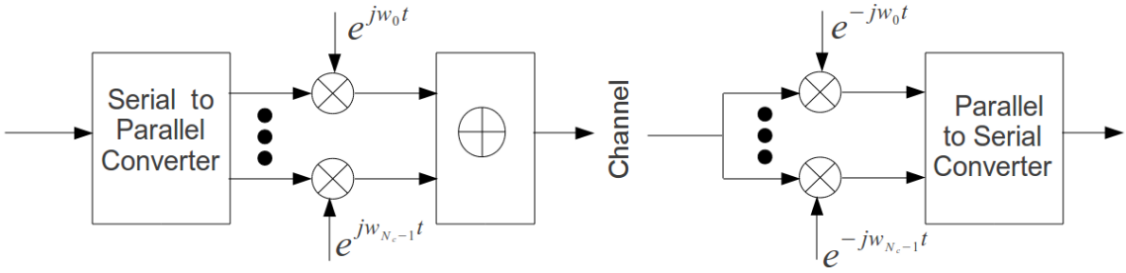

Figure 3.1. OFDM modulator demodulator

$$
\begin{aligned}
&\int_{t_s}^{t_s+T} \exp(-j2\pi\frac{k}{T}(t-t_s)) \sum_{i=-\frac{N_s}{2}}^{\frac{N_s}{2}-1} d_{i+N_s/2}\exp(j2\pi\frac{i}{T}(t-t_s))dt \\
&\quad = \sum_{i=-\frac{N_s}{2}}^{\frac{N_s}{2}-1} d_{i+N_s/2}\exp(j2\pi\frac{i-k}{T}(t-t_s))dt = d_{k+Ns/2}T
\end{aligned} \tag{3.3}
$$

For the k-th demodulated subcarrier, this integration gives the desired output $d_{k+N/2}$ (multiplied by a constant factor T). For all other subcarriers, the integration is zero, because the frequency difference $(i-k)/T$ produces an integer number of cycles within the integration interval T.

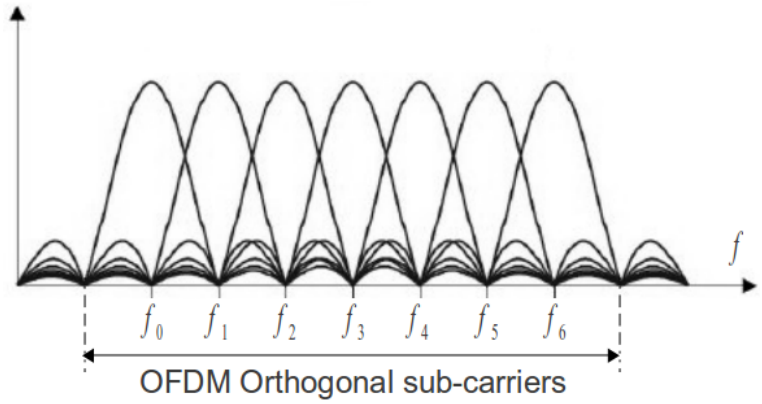

Figure 3.2. Spectra of individual subcarriers

Figures 3.2 shows the typical example of OFDM spectrum. The figure shows seven subcarriers in frequency domain.

Multipath distortion is unavoidable in radio communication systems and the received signal is affected. Although the truncated subchannel sinusoids are delayed by different amounts as channel delays, the distortion is concentrated at the on-off transmissions of these waveforms. Hence, the guard interval is allocated among consecutive OFDM symbols, and Cyclic Prefix (CP) or cyclic extension is placed in the guard interval as shown in Fig. 3.3. The guard interval is set to be longer than the maximal delay spread. The waveform of the tail region of the OFDM signal is copied to the guard interval region. CP eliminates the interference among subcarriers referred to as Inter Carrier Interference (ICI) and between adjacent transmission blocks as an Inter Symbol Interference (ISI). The CP which, in general, is chosen equal to the last part of the OFDM symbol is referred to as cyclic extension.

3.1.2 OFDM Transmitter and Receiver

A block diagram of the baseband of an OFDM transmitter and receiver is shown in Fig. 3.4. The transmitter performs QAM mapping, N_c-point IFFT, and adds a cyclic

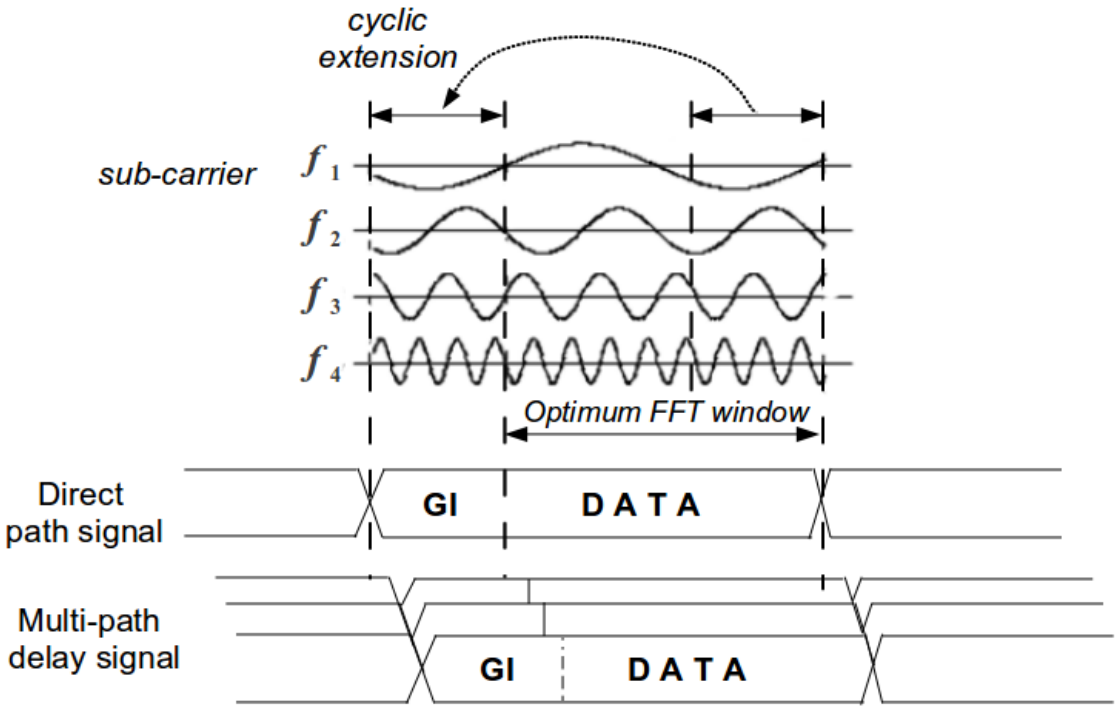

Figure 3.3. OFDM symbol with cyclic prefix

extension before the final TX signal is windowed, transferred to the analogue domain and converted up to the Radio Frequency (RF) and transmitted on air. In order to get an output spectrum with relatively low out-of-band radiation, the size of the IFFT can be chosen larger than the number of subcarriers that is actually used for transmission. For reliable detection, it is, in general, necessary that the receiver know the situation of the wireless communication channel and keep track of phase and amplitude drifts. To enable estimation of the wireless communication channel, the transmitter occasionally sends known training symbols. In Wireless Local Area Networks (WLANs) a preamble, which includes channel training sequences, is added to every packet. Pilot symbols are inserted to every OFDM data symbol on predefined subcarriers.

3.2. MIMO-OFDM System

In order to deal with the frequency-selective nature of wideband wireless channels, MIMO can be combined with OFDM. Effectively, OFDM transforms a frequency-

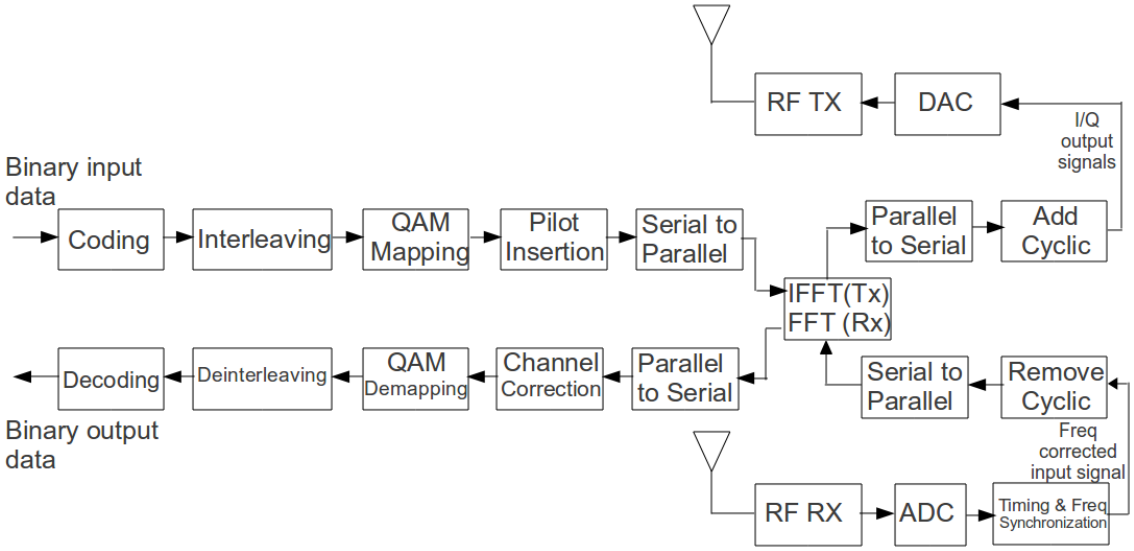

Figure 3.4. OFDM symbol with cyclic prefix

selective channel into parallel flat-fading subchannels, hence the signals on the subcarriers undergo narrowband fading. Hence, by performing MIMO transmission and detection per subcarrier, MIMO algorithms can be applied to broadband wireless communication systems. Now let us suppose MIMO-OFDM system with N_t transmitter (TX) and N_r receiver (RX) antennas. In addition to the spatial and temporal dimension of MIMO, OFDM adds one extra dimension to exploit, namely, the frequency dimension. Block diagram of a MIMO-OFDM transmitter can be envisioned as presented in Fig. 3.5. In general, the incoming bit stream is first encoded by a one-dimensional encoder after which the encoded bits are mapped onto the three available dimensions by the Space-Time- Frequency (STF) mapper. After the STF mapper, each TX branch consists of almost an entire OFDM transmitter.

Block diagram of a MIMO-OFDM receiver is illustrated in Fig. 3.6. After a digital representation of the N_r received signals are obtained by the Analog to Digital Converters (ADC), the receiver first estimates and compensates for the frequency offset and retrieve the symbol timing. Note that it is convenient for the remaining processing to have all receiver branches jointly synchronized and, therefore, the synchronization task should not be performed in parallel per branch, but jointly. Furthermore, for proper frequency synchronisation of the multiple branches it is beneficial to have all branches

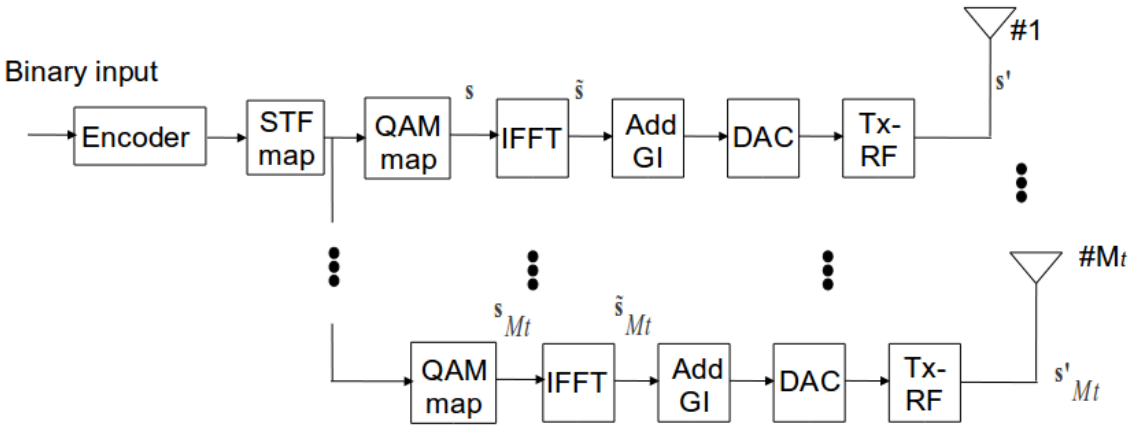

Figure 3.5. Block diagram of a MIMO-OFDM transmitter

at one end of the communication link connected to the same local oscillator in a homodyne structure, or to the same local oscillators providing the multiple frequency levels in a heterodyne structure.

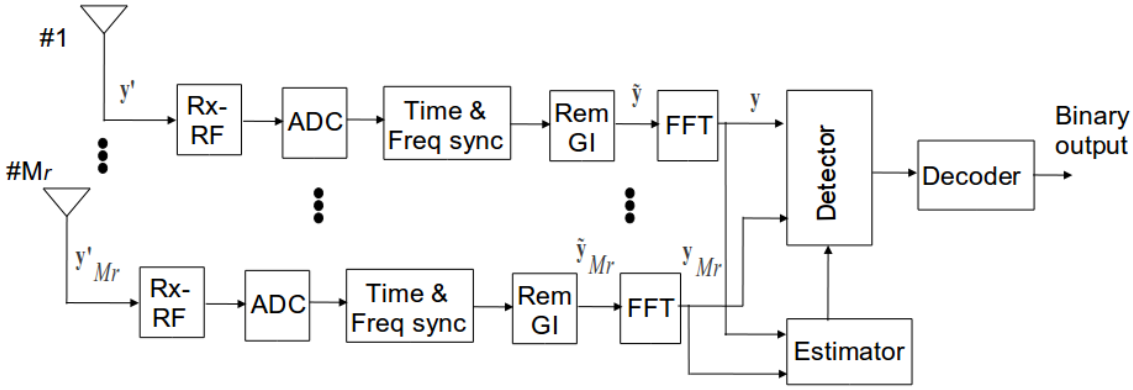

Figure 3.6. Block diagram of a MIMO-OFDM receiver

After synchronisation, the guard interval (GI) is removed and the N_c-point FFT is carried out for all the branches. The received signals corresponding to i-th subcarrier are routed to the i-th MIMO detector to recover the N_t QAM symbols transmitted on that subcarrier. Next, the symbols per TX stream are combined and, finally, STF demapping/ deinterleaving and decoding are performed on these N_t parallel streams and the resulting data are combined to obtain the binary output data. For reliable detection, it is typically necessary that the receiver know the wireless communication

channel and keep track of phase and amplitude drifts. In order to estimate the channel response, the transmitter occasionally sends known training symbols. In WLANs, a preamble, which includes channel-training sequences, is transmitted before sending the data. Moreover, to track the phase drift, pilot symbols are inserted into the predefined subcarriers of every MIMO-OFDM data symbols. Finally, note that OFDM has advantage that it introduces a certain amount of parallelism by means of its N_c subcarriers. This fact can be exploited by MIMO-OFDM. Namely, if MIMO detection is performed per subcarrier, then a given detector is allowed to work N_c times slower than the MIMO detector of an equivalent single carrier system with comparable data rate. Although in the case of MIMO-OFDM N_c of such detectors are required, they can work in parallel, which might make the implementation better.

3.3. MIMO-OFDM Signal Model

In this section, a signal model is introduced for a MIMO-OFDM system in which the relation between the transmitted and received MIMO-OFDM symbols is captured in matrix form. With this concise matrix notation it is shown mathematically that the signal model per subcarrier is equal the narrowband signal model. The strength of this matrix signal model is that it allows for mathematical evaluations of MIMO-OFDM systems, including the outage performance and space-frequency analysis of this chapter. To describe MIMO-OFDM signal model I refer to [9]. The block diagram of MIMO-OFDM transceiver is shown as Figs.3.5 and 3.6.

3.3.1 SISO-OFDM Signal Model

The SISO-OFDM model is first described. This means the system uses a single element antennas at both the receiver and transmiter ($M_R = M_T = 1$). The channel impulse response is given by $g[l]$ where $l = 0, 1, \cdots, L-1$, and L is channel length. The transmitted data symbol s is given by

$$s = [s[0]\ s[1]\ \cdots s[N-1]]^T \tag{3.4}$$

The data symbol is applied to the IFFT processor. This yields the vector

$$\tilde{s} = [\tilde{s}[0]\ \tilde{s}[1]\ \cdots \tilde{s}[N-1]]^T \tag{3.5}$$

This process can be accomplished by

$$\tilde{s} = \mathbf{D}^H \mathbf{s} \tag{3.6}$$

and

$$\mathbf{D} = \frac{1}{\sqrt{N}} \begin{pmatrix} 1 & 1 & 1 & \cdots & 1 \\ 1 & W_N & W^2 & \cdots & W_N^{N-1} \\ \vdots & \vdots & \vdots & \ddots & \vdots \\ 1 & W_N^{N-1} & W_N^{2(N-1)} & \cdots & W_N^{(N-1)^2} \end{pmatrix} \tag{3.7}$$

where $W_N = e^{-j2\pi/N}$.

At the receiver side, the receiver gets a vector $\mathbf{y}'$. And after in GI remover process I obtain N samples of the received signal, $\tilde{\mathbf{y}} = [y'[0]\, y'[1] \cdots y'[N-1]]^T$ are obtained. The received signal vector is given by

$$\tilde{\mathbf{y}} = \tilde{\mathbf{G}}\mathbf{s}' + \tilde{\mathbf{n}} \tag{3.8}$$

where $\tilde{\mathbf{G}}$ is $Nx(N + L - 1)$ circular matrix derived from the channel impulse response and it is given by

$$\tilde{\mathbf{G}} = \begin{pmatrix} g[L-1] & \cdots & g[1] & g[0] & 0 & 0 & \cdots & 0 \\ 0 & g[L-1] & \cdots & g[1] & g[0] & 0 & \cdots & 0 \\ \vdots & 0 & \ddots & \ddots & \ddots & \ddots & \ddots & \vdots \\ 0 & \vdots & 0 & g[L-1] & \cdots & g[1] & g[0] & 0 \\ 0 & 0 & 0 & 0 & g[L-1] & \cdots & g[1] & g[0] \end{pmatrix} \tag{3.9}$$

The last $(L-1)$ samples of transmitted sequence of $\mathbf{s}'$ are identical to the first $(L-1)$ samples of the Guard Interval Adder, then I can simplify equation (3.8) as

$$\tilde{\mathbf{y}} = \tilde{\mathbf{G}}_h \tilde{\mathbf{s}} + \tilde{\mathbf{n}} \tag{3.10}$$

where

$$\tilde{\mathbf{G}}_{\mathbf{h}} = \begin{pmatrix} g[0] & 0 & \cdots & 0 & 0 & g[L-1] & \cdots & g[1] \\ g[1] & g[0] & 0 & \cdots & 0 & 0 & \ddots & \vdots \\ \vdots & g[1] & g[0] & 0 & 0 & \ddots & 0 & g[L-1] \\ g[L-1] & \vdots & g[1] & \ddots & 0 & \ddots & 0 & 0 \\ 0 & g[L-1] & \vdots & \ddots & g[0] & \ddots & \ddots & 0 \\ \vdots & 0 & g[L-1] & \ddots & g[1] & g[0] & 0 & 0 \\ \vdots & \vdots & 0 & \ddots & \vdots & \ddots & \ddots & 0 \\ 0 & 0 & \cdots & 0 & g[L-1] & \cdots & g[1] & g[0] \end{pmatrix} \tag{3.11}$$

The Guard Interval (GI) adder gives the matrix $\mathbf{G}_h$ circulant which can be expressed by

$$\mathbf{G}_h = \mathbf{D}^H \mathbf{\Omega} \mathbf{D} \tag{3.12}$$

where

$$\mathbf{\Omega} = \begin{pmatrix} \omega[0]] & 0 & 0 & 0 & 0 \\ 0 & \omega[1] & 0 & 0 & 0 \\ 0 & 0 & \omega[2] & 0 & 0 \\ 0 & 0 & 0 & \ddots & 0 \\ 0 & 0 & 0 & 0 & \omega[N-1 \end{pmatrix} \tag{3.13}$$

and

$$\omega[k] = \sum_{l=0}^{L-1} g[l] e^{-\frac{j2\pi kl}{N}} \tag{3.14}$$

where k is tone index; $k = 0, 1, \cdots, N-1$. The received signal is applied to the FFT. The output of the FFT is given by

$$\mathbf{y} = \mathbf{D}\tilde{\mathbf{y}} \tag{3.15}$$

where $\mathbf{y} = [y[0]\ y[1]\ y[2]\ \cdots\ y[N-1]]$. Using the equations (3.6),(3.10),(3.12) and (3.15), The received signal before and after FFT are rewritten respectively as

$$\begin{aligned} \tilde{\mathbf{y}} &= \mathbf{G}_h \tilde{\mathbf{s}} + \tilde{\mathbf{n}} \\ &= \mathbf{G}_h \left(\mathbf{D}^H \mathbf{s} \right) + \tilde{\mathbf{n}} \\ &= \mathbf{D}^H \mathbf{\Omega} \mathbf{D} [\mathbf{D}\mathbf{s}] + \tilde{\mathbf{n}} \end{aligned} \tag{3.16}$$

and

$$\begin{aligned} \mathbf{y} &= \mathbf{D}\tilde{\mathbf{y}} \\ &= \mathbf{D}\mathbf{D}^H\Omega\mathbf{D}(\mathbf{D}^H s) + \tilde{\mathbf{n}} \\ &= \mathbf{D}\mathbf{D}^H\Omega\mathbf{D}\mathbf{D}^H\mathbf{s} + \mathbf{D}\tilde{\mathbf{n}} \\ &= \mathbf{\Omega}\mathbf{s} + \mathbf{n} \end{aligned} \tag{3.17}$$

Since $\mathbf{\Omega}$ is a diagonal matrix, the k-th subcarrier component of Equation (3.18) is given by

$$y[k] = \omega[k]s[k] + n[k] \tag{3.18}$$

where $n[k]$ is the k-th element of noise, $\mathbf{n}$; $k = 0, 1, 2, \cdots, (N-1)$.

3.3.2 MIMO-OFDM Signal Model

The SISO-OFDM signal model has been described in the previous section. In this section, MIMO-OFDM systems are explained. A frequency selective MIMO channel with M_T transmitter antennas, M_R receiver antennas is assumed. The channel impulse response is assumed to be $g_{i,j}[l]$, where $l = 0, 1, \cdots, L-1$ and L is the maximum channel length, i, j are ith receive antenna ($i = 1, 2, \cdots, M_R$) and j-th transmitte antenna ($j = 1, 2, \cdots, M_T$). Let the sequence be transmitted over the j-th transmitter antenna be $s_j[k]$, where $k = 0, 1, 2, \cdots, N-1$. Similarly to the SISO-OFDM system, the signal received at the i-th receive antenna over the k-th subcarrier, $y_i[k]$; and $k = 0, 1, 2, \cdots, N-1$ is given by

$$y_i[k] = \sqrt{\frac{1}{M_T}} \sum_{j=1}^{M_T} \omega_{i,j}[k]s_j[k] + n_i[k] \tag{3.19}$$

where i is i-th receiver antenna ($1, 2, .. \cdots, M_R$) and $n_i[k]$ is a noise with variance N_0 and $\omega_{i,j}[k]$ is the channel gain between the j-th transmitter antennas. And $\omega_{i,j}[k]$ is shown as

$$\omega_{i,j}[k] = \sum_{l=0}^{L-1} g_{i,j}[l]e^{-\frac{j2\pi kl}{N}} \tag{3.20}$$

where k is tone index; $k = 0, 1, \cdots, N-1$. From the equation (3.19) I can show the MIMO channel response for the k-th subcarrier can be shown as:

$$\mathbf{y}[k] = \sqrt{\frac{1}{M_T}}\mathbf{H}[\mathbf{k}]\mathbf{s}[k] + \mathbf{n}[k] \tag{3.21}$$

where $\mathbf{y}[k] = [y_1[k]\ y_2[k]\ \cdots y_{M_R}[k]]^T$, $\mathbf{n}[k] = [n_1[k]\ n_2[k]\ \cdots n_{M_R}[k]]^T$ and $\mathbf{H}[k]$ is $M_R \times M_T$ matrix with $[\mathbf{H}[k]]_{i,j} = \omega_{i,j}[k]$. The matrix $\mathbf{H}[k]$ is the frequency response of the matrix channel corresponding to the k-th tone and is related to $\mathbf{G}[l]$. And G is from $\mathbf{H}[k] = \sum_{l=0}^{L-1} \mathbf{G}[l]e^{-\frac{j2\pi kl}{N}}$.

Chapter 4

An RF Signal Processing Based Diversity Receiver for the SISO-OFDM System

IN this section, I will briefly introduce the RF signal processing based diversity receiver for the SISO-OFDM system.

4.1. Block diagram

Figure 4.1 illustrates the receiver block diagram of the SISO-OFDM system using RF signal processing. The RF signal processing in this scheme is composed of a phase non-shifting element and a phase shifting element terminated with a variable capacitor. Since the phase non-shifting element and the phase shifting element are electromagnetically coupled, the output of the RF signal processing is the weighted sum of the received signal at each element [10].

Figure 4.2 shows the frequency spectrum of the transmitted and the received signals. Figure 4.2(a) is the frequency spectrum of the transmitted signal. Subcarriers are divided into two groups and allocated to the positive and negative sides of the frequency band. The frequency spectrum of the received signal at the output of the phase shifting element is illustrated in Fig. 4.2(b), whose frequency is positive frequency shifted for subcarrier frequency spacing. The received signal is composed of

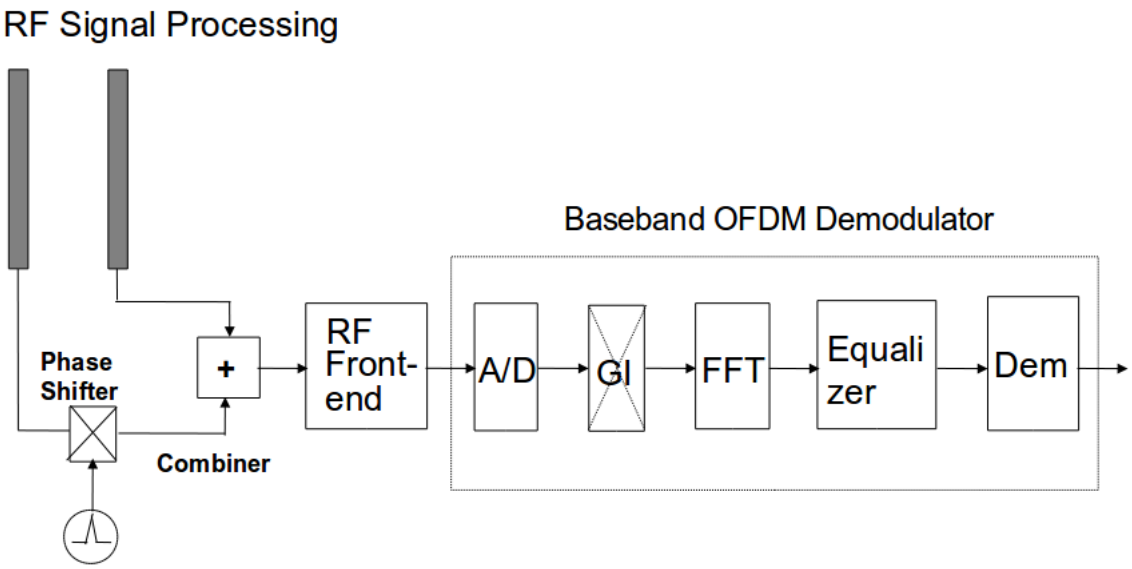

Figure 4.1. Block diagram of the SISO-OFDM receiver with RF signal processing

the shifted and the non-shifted signal components as shown in Fig. 4.2(c), the overall number of efficient subcarriers are N+2, where N is the number of subcarriers.

Now, let $v_d(t)$ and $v_p(t)$ be the received signals corresponding to the phase non-shifting and the phase shifting elements respectively.

In this scheme the phase shifter is controlled by the oscillator whose frequency is the same as the subcarrier spacing of the OFDM signal. Then the output of the RF signal processing is given by

$$v(t) = \alpha v_d(t) + \beta e^{\frac{j2\pi t}{T_s}} v_p(t), \tag{4.1}$$

where T_s is a FFT (Fast Fourier Transform) window period of the OFDM signal, while α and β are weighting factors for the phase non-shifting element and the phase shifting element. At the receiver, a specific type of equalization is required to reduce the ICI (Inter Channel Interference) generated by the proposed scheme. In the following, let me derive the channel estimation algorithm for the proposed RF signal processing based diversity receiver. The received signal is applied to the FFT processor followed by the frequency-domain equalizer.

Now let us assume that the transmitted symbol vector in the frequency-domain is

$$\mathbf{x} = [x_0, x_1, \cdots, x_{N-1}]^T, \tag{4.2}$$

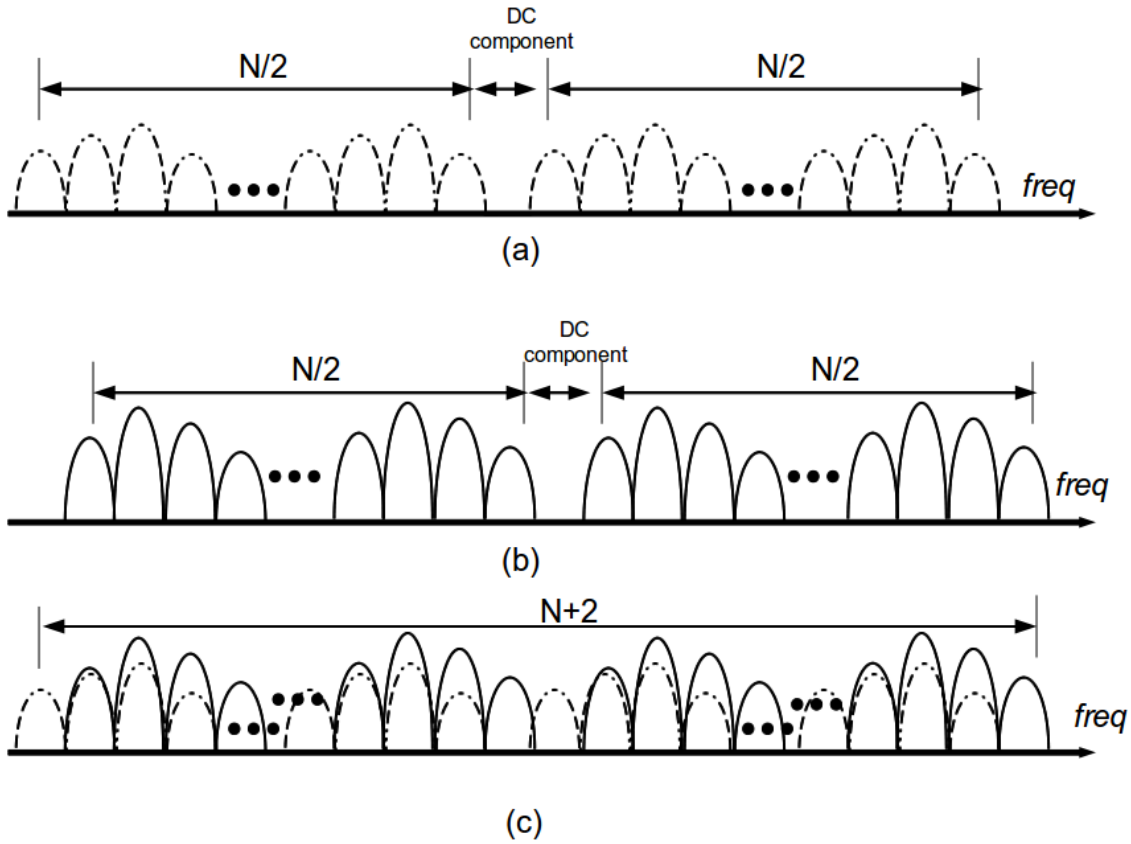

Figure 4.2. The frequency spectrum of transmitted and received signals. (a) In the transmitter, (b) In the phase shifting element of receiver, and (c) In the combiner of receiver

where x_k is the data symbol of the k-th subcarrier. The transmitted symbol vector is divided into two parts, and zeros are padded to adjust the vector size to FFT window. The modified transmitted vector is given by

$$\hat{x} = \left[0 \,\middle|\, x_0\ x_1\ \cdots\ x_{N/2-1} \,\middle|\, 0_{N_{FFT}-N-1} \,\middle|\, x_{N/2}\ \cdots\ x_{N-1}\right]^T, \tag{4.3}$$

where N_{FFT} is the FFT window size.

The data symbol in the time-domain is given by

$$\mathbf{v} = \mathbf{F}^{-1}\hat{\mathbf{x}}, \tag{4.4}$$

where $\mathbf{F}$ is the Fourier transformation matrix. That is, the k-th column l-th raw element of $\mathbf{F}$ is $e^{-j\frac{2\pi kl}{N_{FFT}}}$. The transmitted symbol $\mathbf{v}$ is then propagated through the multipath

fading channel. The received signal component at the i-th element is given by

$$\mathbf{q}_i = \mathbf{C}_i \mathbf{v}, \tag{4.5}$$

where $\mathbf{C}_i$ is the channel impulse response matrix corresponding to the i-th element. The received signal at the input of the baseband demodulation block is given by

$$\begin{aligned} \mathbf{r} &= \mathbf{q}_i + \mathbf{D}\mathbf{q}_{i+1} + \mathbf{z}_T \\ &= (\mathbf{C}_1 + \mathbf{D}\mathbf{C}_2)\,\mathbf{v} + \mathbf{z}_T \\ &= (\mathbf{C}_1 + \mathbf{D}\mathbf{C}_2)\,\mathbf{F}^{-1}\mathbf{x} + \mathbf{z}_T, \end{aligned} \tag{4.6}$$

where $\mathbf{z}_T$ is the thermal noise component in the time-domain, and $\mathbf{D} = \text{diag}\{d_0, \cdots d_{N-1}\}$ is a diagonal matrix, whose k-th diagonal element is d_k. According to (4.1), d_k is given by

$$d_k = e^{j\frac{2\pi k}{N_{FFT}}}. \tag{4.7}$$

The received signal is applied to the FFT. The output of the FFT is then given by

$$\hat{\mathbf{u}} = \mathbf{F}\mathbf{r} = \left(\hat{\mathbf{H}}_1 + \hat{\mathbf{G}}\hat{\mathbf{H}}_2\right)\hat{\mathbf{x}} + \hat{\mathbf{z}}, \tag{4.8}$$

where $\hat{\mathbf{z}} = \mathbf{F}\,\mathbf{z}_T$ is the thermal noise component in the frequency-domain. And

$$\hat{\mathbf{H}}_i = \mathbf{F}\mathbf{C}_i\mathbf{F}^{-1}, \tag{4.9}$$

is a diagonal matrix ($i = 1, 2$), whose diagonal elements represent the frequency response.

$$\hat{\mathbf{G}} = \mathbf{F}\mathbf{D}\mathbf{F}^{-1}, \tag{4.10}$$

represents the ICI matrix in the frequency-domain.

I can further reduce (4.8) by removing the elements without data symbols as

$$\mathbf{u} = (\mathbf{H}_1 + \mathbf{G}\mathbf{H}_2)\,\mathbf{x} + \mathbf{z}, \tag{4.11}$$

where

$$\mathbf{u} = \left[\hat{u}_1\ \hat{u}_2\ \cdots \hat{u}_{N/2} \,\middle|\, \hat{u}_{N_{FFT}-N/2-1}\ \cdots\ \hat{u}_{N_{FFT}-1}\right], \tag{4.12}$$

$$\mathbf{G} = \begin{bmatrix} \hat{G}(1:\frac{N}{2}+1, 1:\frac{N}{2}) & \text{zeros}(\frac{N}{2}+1, \frac{N}{2}) \\ \text{zeros}(\frac{N}{2}+1, \frac{N}{2}) & \hat{G}(a_G : N_{FFT}, a_G : N_{FFT}-1) \end{bmatrix}, \tag{4.13}$$

where $a_G = N_{FFT} - N/2$, and

$$\mathbf{H}_i = \begin{bmatrix} \hat{H}_i(d_H : e_H, a_H : b_H) & \text{zeros}(\frac{N}{2}, \frac{N}{2}) \\ \text{zeros}(1, N) & \\ \text{zeros}(\frac{N}{2}, \frac{N}{2}) & \hat{H}_i(g_H : h_H, b_H + 2 : c_H + 1) \end{bmatrix}, \tag{4.14}$$

where $a_H = (N_{FFT} - N + 2)/2$, $b_H = N_{FFT}/2$, $c_H = (N_{FFT} - 4)$, $d_H = a_H - 1 + i$, $e_H = b_H - 1 + i$, $g_H = b_H + 1 + i$, $h_H = c_H + i$, and $i = 1, 2$. The operation of zeros (m, n) denote an m-by-n matrix of zeros and $\hat{H}_i(r{:}j, k{:}l)$ is the $\hat{H}_i$ matrix with (r-th until j-th) rows and (k-th until l-th) columns respectively.

4.2. Channel Estimation

According to (4.8), the adjacent subcarrier signals interfere with the received signal. That is, the receiver requires frequency-domain equalization. To equalize the signal, the frequency response of the channel must be estimated. To estimate the frequency response, the sender first transmits a pilot symbol before transmitting the data. Now let us assume that the pilot symbol vector in the frequency-domain is

$$\mathbf{p} = [p_0, p_1, \cdots, p_{N-1}]^T, \tag{4.15}$$

where p_k is the pilot symbol at the k-th subcarrier. The received signal at the pilot symbol is then given by

$$\mathbf{u} = (\mathbf{H}_1 + \mathbf{G}\mathbf{H}_2)\,\mathbf{p} + \mathbf{z}. \tag{4.16}$$

Now, let us assume that the vector $\mathbf{p}$ and $\mathbf{h}_i$ denote the diagonal components of the matrices $\mathbf{P}$ and $\mathbf{H}_i$ respectively. That is,

$$\mathbf{P} = \text{diag}\{p_0, p_1, \cdots, p_{N-1}\}, \tag{4.17}$$

and

$$\mathbf{H}_i = \text{diag}\{\mathbf{h}_1, \cdots, \mathbf{h}_i\}. \tag{4.18}$$

Then without loss of generality, can be exchanged the diagonal matrices and vectors as in

$$\mathbf{u} = \mathbf{P}\mathbf{h}_1 + \mathbf{G}\mathbf{P}\mathbf{h}_2 + \mathbf{z}. \tag{4.19}$$

The auto-correlation ($\mathbf{R}$) and cross-correlation ($\mathbf{B}$) matrices are now derived as follows.

$$\begin{aligned}
\mathbf{R} &= E\left[\mathbf{u}\mathbf{u}^H\right] \\
&= E\left[(\mathbf{P}\mathbf{h}_1 + \mathbf{G}\mathbf{P}\mathbf{h}_2 + \mathbf{z})(\mathbf{P}\mathbf{h}_1 + \mathbf{G}\mathbf{P}\mathbf{h}_2 + \mathbf{z})^H\right] \\
&= E\left[(\mathbf{P}\mathbf{h}_1 + \mathbf{G}\mathbf{P}\mathbf{h}_2 + \mathbf{z})(\mathbf{P}\mathbf{h}_1)^H\right] + \\
&\quad E\left[(\mathbf{P}\mathbf{h}_1 + \mathbf{G}\mathbf{P}\mathbf{h}_2 + \mathbf{z})(\mathbf{G}\mathbf{P}\mathbf{h}_2)^H\right] + \\
&\quad E\left[(\mathbf{P}\mathbf{h}_1 + \mathbf{G}\mathbf{P}\mathbf{h}_2 + \mathbf{z})(\mathbf{z})^H\right] \\
&= \mathbf{P}\mathbf{R}_h\mathbf{P}^H + \mathbf{G}\mathbf{P}\mathbf{R}_h\mathbf{P}^H\mathbf{G}^H + \sigma_Z^2\mathbf{I}, \qquad (4.20)
\end{aligned}$$

where $E[\times]$ is the ensemble average of random variable, $\times$. In the following, let us assume that $\mathbf{h}_1$ and $\mathbf{h}_2$ are uncorrelated. That is,

$$E[\mathbf{h}_1\mathbf{h}_2^H] = 0, \qquad (4.21)$$

and

$$E[\mathbf{h}_1\mathbf{h}_1^H] = E[\mathbf{h}_2\mathbf{h}_2^H] = \mathbf{R}_h, \qquad (4.22)$$

is the covariance matrix of $\mathbf{h}_i$ ($i = 1, 2$), and

$$\mathbf{B}_i = E\left[\mathbf{u}\mathbf{h}_i^H\right]. \qquad (4.23)$$

The cross-correlation matrices for the phase non-shifting element ($\mathbf{B}_1$) and the phase shifting element ($\mathbf{B}_2$) are further given by

$$\mathbf{B}_1 = \mathbf{P}\mathbf{R}_h, \qquad (4.24)$$

and

$$\mathbf{B}_2 = \mathbf{G}\mathbf{P}\mathbf{R}_h. \qquad (4.25)$$

The channel response is finally estimated by

$$\mathbf{h}_i = \mathbf{W}_i^H\mathbf{u}, \qquad (4.26)$$

where

$$\mathbf{W}_i = \mathbf{R}^{-1}\mathbf{B}_i, \qquad (4.27)$$

is the weight matrix in terms of the minimum mean square error (MMSE) criterion, where $\mathbf{R}^{-1}$ is the inverse matrix of $\mathbf{R}$.

4.3. Frequency-domain Equalizer

From the estimated channel response, the received data symbols can be equalized. In the following is assumed a straightforward ZF (Zero Forcing) equalizer. The estimated value of the transmitted symbol is given by

$$\tilde{\mathbf{x}} = \left(\tilde{\mathbf{H}}_\mathbf{1} + \mathbf{G}\tilde{\mathbf{H}}_\mathbf{2}\right)^{+} \mathbf{u}, \tag{4.28}$$

where $\tilde{\mathbf{H}}_i$ is the estimated channel response.

Chapter 5

The Proposed RF Signal-processing-based MIMO-OFDM System

THE proposed MIMO-OFDM system with RF signal processing is an extension of the RF signal processing based diversity receiver proposed in the previous work [6]. In this section let me present a 2×2 MIMO-OFDM system with RF signal processing. The transmitter and receiver block diagrams of the proposed MIMO-OFDM systems with RF signal processing are shown in Figs. 5.1 and 5.2. Figure 5.1 represents the pilot symbol transmission phase of the MIMO-OFDM transmitter. As introduced in the MIMO-OFDM WLAN (Wireless Local Area Network) standard in IEEE 802.11n [11], the pilot tone for the second stream of the transmitter is shifted by a CS (Cyclic Shift) block. The signals are then applied to the corresponding Mod (Modulator), IFFT processor, GI (Guard Interval) adder, D/A (Digital to Analog) converter and HPA (High Processor Amplifier) respectively for further transmission by transmitter antenna. At the receiver as shown in Fig. 5.2, use two RF signal processing to receive the signal. The received signals are then applied to the corresponding A/D (Analog to Digital) converter, GI (Guard Interval) remover and FFT processors respectively, followed by the channel estimator and MIMO decoder. The output of the MIMO decoder is then applied to the demapper to demodulate the symbol.

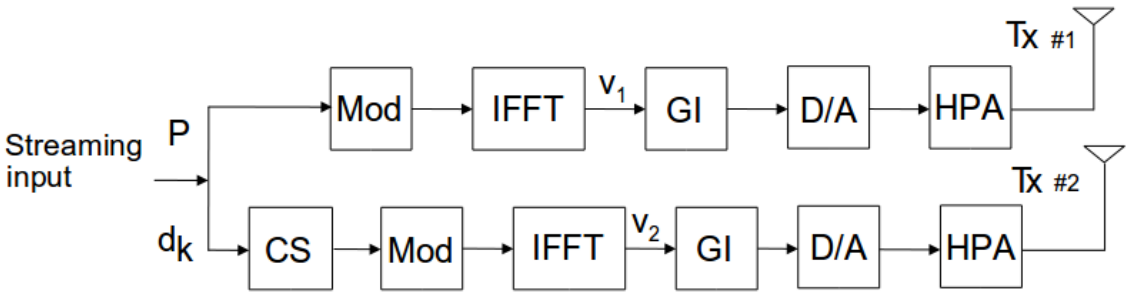

Figure 5.1. Block diagram of the MIMO-OFDM transmitter

5.1. Channel Estimation

Let the pilot symbol and its cyclic shifted one be $\mathbf{P_1}$ and $\mathbf{P_2}$ respectively. The received signal $\mathbf{u}_i$ calculated as in [6] at the i-th RF signal processing in the frequency-domain is given by

$$\begin{aligned} \mathbf{u}_i &= \mathbf{P}_1\mathbf{h}_{i,1}^{ns} + \mathbf{G}\mathbf{P}_1\mathbf{h}_{i,1}^{s} \\ &\quad + \mathbf{P}_2\mathbf{h}_{i,2}^{ns} + \mathbf{G}\mathbf{P}_2\mathbf{h}_{i,2}^{s} + \mathbf{z}, \end{aligned} \tag{5.1}$$

where $\mathbf{h}_{i,l}^{ns}$ and $\mathbf{h}_{i,l}^{s}$ are the channel response between the i-th receiver antenna element and l-th transmitter antenna element for the phase non-shifting element (ns) and the phase shiting element (s), respectively.

By using $\mathbf{R} = E[\mathbf{u}_i\mathbf{u}_i^H]$ and $\mathbf{B}_i = E[\mathbf{u}\,\mathbf{h}^H]$ for auto-correlation and cross-correlation respectively, then from (5.1), the auto-correlation matrix can be obtained by

$$\begin{aligned} \mathbf{R} &= \mathbf{P_1}\mathbf{R}_h\mathbf{P}_1^H + \mathbf{G}\mathbf{P_1}\mathbf{R}_h\mathbf{P}_1^H\mathbf{G}^H \\ &\quad + \mathbf{P_2}\mathbf{R}_h\mathbf{P_2^H} + \mathbf{G}\mathbf{P_2}\mathbf{R}_h\mathbf{P_2^H}\mathbf{G}^H + \sigma_{\mathbf{z}}^{\mathbf{2}}\mathbf{I}, \end{aligned} \tag{5.2}$$

and cross-correlation is given by

$$\begin{aligned} \mathbf{B}_i^{ns} &= \mathbf{P_i}\mathbf{R}_h, \\ \mathbf{B}_i^{s} &= \mathbf{G}\mathbf{P_i}\mathbf{R}_h, \end{aligned} \tag{5.3}$$

where $i = 1, 2$. $\mathbf{B}_i^{ns}$ and $\mathbf{B}_i^{s}$ are a cross-correlation matrix in i-th receiver antenna element for the phase non-shifting element (ns) and the phase shifting element (s) respectively.

In this research a rectangular shaping filter for the Rayleigh fading channel model is used. In this section, it is described in detail. Considering Fig. 5.3, following equation can be given

$$p(\tau) = \begin{cases} 1; & 0 \leq \tau \leq T_1 \\ 0; & \text{otherwise} \end{cases}, \tag{5.4}$$

for time domain. And for frequency domain, the covariance matrix is given as follows.

$$\begin{aligned} \mathbf{R}(\Delta_f) &= \int_0^{\infty} p\tau e^{-j2\pi\Delta_f\tau} d\tau \\ &= \int_0^{\infty} e^{-j2\pi\Delta_f\tau} d\tau \\ &= \left[\frac{e^{-j2\pi\Delta_f\tau}}{-j2\pi\Delta_f\tau} \right]_0^{T_1} \\ &= \frac{1 - e^{-j2\pi\Delta_f T_1}}{j2\pi\Delta_f T_1} \\ &= e^{-j\pi\Delta_f T_1} \frac{e^{j\pi\Delta_f T_1} - e^{-j\pi\Delta_f T_1}}{j2\pi\Delta_f T_1} \end{aligned} \tag{5.5}$$

To realize this equation, it can be modified as shown in (5.6).

$$\mathbf{R}_h(k) = e^{-j\pi\Delta_f T_1} \frac{sin\left(\pi\Delta_f T_1(l-k)\right)}{\pi\Delta_f T_1(l-k)}, \tag{5.6}$$

where Δ_f denotes the subcarrier spacing, l, k are l-th row and k-th column with $1, 2, \cdots, N$ and T_1 denotes the root-mean-squared delay spread respectively for the Rayleigh fading channel model.

In this research an exponential shaping filter is used for IEEE 802.11n channel model and WINNER channel model. In this section it is described in detail. Considering Fig. 5.4, following equation can be given

$$p_{ex}(\tau) = \begin{cases} \frac{1}{T_1} e^{-\frac{\tau}{T_1}} & 0 \geq \tau \\ 0 & \text{otherwise} \end{cases}, \tag{5.7}$$

for time domain. And for frequency domain, the covariance matrix is given as follows.

$$\begin{aligned}
\mathbf{R}_{ex}(\Delta_f) &= \int_0^{\infty} p_{ex}(\tau) e^{-j2\pi\Delta_f\tau} d\tau \\
&= \int_0^{\infty} \frac{1}{T_1} e^{-\frac{\tau}{T_1}}\ e^{-j2\pi\Delta_f\tau} d\tau \\
&= \frac{1}{T_1}\int_0^{\infty} e^{-\tau(\frac{1}{T_1}+j2\pi\Delta_f)} d\tau \\
&= -\frac{1}{T_1}\frac{1}{\frac{1}{T_1}+j2\pi\Delta_f} e^{-\tau(\frac{1}{T_1}+j2\pi\Delta_f)}\Big|_0^{\infty} \\
&= \frac{1}{1+j2\pi\Delta_f T_1}.
\end{aligned} \tag{5.8}$$

To realize this equation, it can be modified it as shown in (5.9).

$$\mathbf{R}_h(k) = \frac{1}{1+j2\pi\ \Delta_f\ T_1(l-k)}, \tag{5.9}$$

where Δ_f denotes the subcarrier spacing, l, k are l-th row and k-th column with $1, 2, \cdots, N$ and T_1 denotes the root-mean-squared delay spread respectively for IEEE 802.11n channel model and WINNER channel model.

The channel response for a 2×2 MIMO-OFDM system with RF signal processing corresponding to the first receiver (5.10) and the second receiver (5.11) is finally estimated respectively by

$$\mathbf{h}_{i,l}^{ns} = (\mathbf{W}_{\mathbf{i}}^{\mathbf{ns}})^H \mathbf{u}_i, \tag{5.10}$$

and

$$\mathbf{h}_{i,l}^{s} = (\mathbf{W}_{\mathbf{i}}^{\mathbf{s}})^H \mathbf{u}_i, \tag{5.11}$$

where $i = 1, 2$; $l = 1, 2$. And the weight matrix $\mathbf{W}$ is given by

$$\begin{aligned}
\mathbf{W}_i^{ns} &= \mathbf{R}^{-1}\mathbf{B}_i^{ns}, \\
\mathbf{W}_i^{s} &= \mathbf{R}^{-1}\mathbf{B}_i^{s}.
\end{aligned} \tag{5.12}$$

5.2. MIMO Decoding

After the estimation of channel response, MIMO decoding is carried out. In the following I use a V-BLAST based algorithm, which simultaneously performs both the

MIMO decoding and frequency-domain equalization for RF signal processing. Let us describe the three schemes for MIMO detection using n V-BLAST processors (n = 1, 2 and 4) as follows.

5.2.1 MIMO Detection Using 1 V-BLAST Processor

In the following, the number of subcarriers used for data transmission is assumed N. Similar to the RF signal processing based diversity receiver in Sec. 4, the ICI is generated at the RF signal processing section. According to Fig. 4.2(c), the number of received symbols is N+2.

The block diagram of the MIMO decoder using 1 V-BLAST processor is shown in Fig. 5.5. The V-BLAST processor performs MIMO decoding and frequency-domain equalization simultaneously. The channel matrices frequency components are given by (5.14) where $\mathbf{H}_{i,j}$ is the channel matrix for a receiver j from transmitter i, and the size of each matrix is $(N+2) \times N$, hence the size of matrix $\mathbf{H}$ is $2(N+2) \times 2N$. $\mathbf{H}_{ij}$ is shown in (5.13).

$$\mathbf{H} = \begin{pmatrix} \mathbf{H}_{1,1} & \mathbf{H}_{1,2} \\ \mathbf{H}_{2,1} & \mathbf{H}_{2,2} \end{pmatrix}. \tag{5.14}$$

In the V-BLAST detection algorithms [7] and [12], the symbols are first detected using a linear process such as ZF or MMSE. The detected symbols are regenerated, and the corresponding signal portion is subtracted from the received signal vector with the fewest interfering signal components. This process is repeated, until all N symbols are detected [7]. The detection process using V-BLAST algorithms is illustrated in Table 5.1. From this table the procedure of V-BLAST detection for our scheme is as follows.

Let $\mathbf{a} = [a_1, a_2, \cdots, a_{2(N+2)}]^T$ be the transmitted symbol vector, then the received symbol is $\mathbf{r} = \mathbf{Ha} + \mathbf{z}$ where $\mathbf{H}$ is either one of the channel matrices given in (5.14) and $\mathbf{z}$ is a noise vector. Assuming that $\mathbf{S} = \{m_1, m_2, \cdots, m_{2N}\}$ denotes a sequence of substream received data. As an initialization, I set $\mathbf{H}_1 = \mathbf{H}$, where the size of the channel matrix is $2(N+2) \times 2N$, $\mathbf{r} = \mathbf{r}_1$ and $i = 1$.

The following steps are repeated until all substreams are detected :

- Compute $\mathbb{G}= \mathbf{H}_i^+$ and select substream as m_i

- Use the equalization vector $\mathbf{w}_{m_i}$ to yield $\mathbf{y}_{m_i}$
- Make a decision based on $\mathbf{y}_{m_i}$ to get the estimation $\hat{\mathbf{a}}_{m_i}$
- Assuming that $\hat{\mathbf{a}}_{m_i}$ is correct, cancel $\hat{\mathbf{a}}_{m_i}$ from $\mathbf{r}_i$ to get $\mathbf{r}_{i+1}$
- Obtain the modified channel matrix $\mathbf{H}_{i+1}$ by removing the m_i-th column of $\mathbf{H}_i$, and set $i = i + 1$

Table 5.1. V-BLAST detection algorithms

Initialization	Recursion
$i \leftarrow 1$	$\mathbf{w}_{mi} = (\mathbb{G}_i)_{mi}$
$\mathbb{G}_1 = \mathbf{H}^+$	$\mathbf{y}_{mi} = \mathbf{w}_{mi}\mathbf{r}_i$
$m_1 = \underbrace{\arg\min}_{j} \|(\mathbb{G}_1)_j\|^2$	$\hat{\mathbf{a}}_{m_i} = \mathbf{Q}(\mathbf{y}_m)_i$
	$\mathbf{r}_{i+1} = \mathbf{r}_i - \hat{\mathbf{a}}_{m_i}\mathbf{H}_{m_i}$-
	$\mathbb{G}_{i+1} = \mathbf{H}^+{}_{m_i}$
	$m_{1+1} = \underbrace{\arg\min}_{j \notin \{m_1, m_2, \cdots, m_i\}} \|(\mathbb{G}_{i+1})_j\|^2$
	$i \leftarrow i + 1$

5.2.2 MIMO Detection Using 2 V-BLAST Processors

In this section let me modify the channel matrix size to one half of the original channel matrix size. The channel matrix is shown in (5.15) and (5.16) for upper channel matrices ($\mathbf{H}_{up}$) and lower channel matrices ($\mathbf{H}_{lo}$) with $(N + 2) \times N$ matrix size respectively. The upper channel matrices correspond to the phase non-shifting element and the lower channel matrices correspond to the phase shifting element. These channel matrices are applied in each V-BLAST processor. Figure 5.6 shows a MIMO decoder using 2 V-BLAST processors.

5.2.3 MIMO Detection Using 4 V-BLAST Processors

In this section, let me modify the channel matrix size to one quarter of the original channel matrix size. The channel matrix is shown in (5.17) and (5.18) for upper channel matrices ($\mathbf{H}_{uA}$) and ($\mathbf{H}_{uB}$), and in (5.19) and (5.20) for lower channel matrices ($\mathbf{H}_{lA}$) and ($\mathbf{H}_{lB}$) with $(N/2 + 2) \times N/2$ matrix size respectively. The upper channel matrices correspond to the phase non-shifting element and the lower channel matrices correspond to the phase shifting element. These channel matrices are

applied in each V-BLAST processor. Figure 5.7 shows a MIMO decoder using 4 V-BLAST processors.

5.3. Evaluation of MIMO Detection Using n V-BLAST Processors

MIMO detection using 1 V-BLAST processor with the original size was described above; however, the computations became too complex and required a long processing time, so I must simplify the size of the V-BLAST processor. Two scenarios for reducing the computational cost and complexity. The first scheme : the size of the matrix is half of the original channel matrix size requiring 2 V-BLAST processors. The second scheme : the size of the matrix is a quarter of the original channel matrix size requiring 4 V-BLAST processors. From the computer simulation, using 1 V-BLAST processor and 2 V-BLAST processors, the performance of the system is almost the same, but the computational time with 2 processors is less than that of 1 processor. However, because the inter channel interference (ICI) from the adjacent segments cannot be cancelled by the corresponding V-BLAST processors and this information is not informed by the corresponding V-BLAST processors, the performance of the system using 4 V-BLAST processors is very bad (SNR is very large or infinite), so attempting to use a channel matrix a quarter of the size of the original channel matrix is not worthwhile. Figure 5.8 shows the curve of error performances (at $BER = 10^{-3}$) for n V-BLAST processors. So I decided to use a V-BLAST algorithm with 2 processors for the MIMO detection.

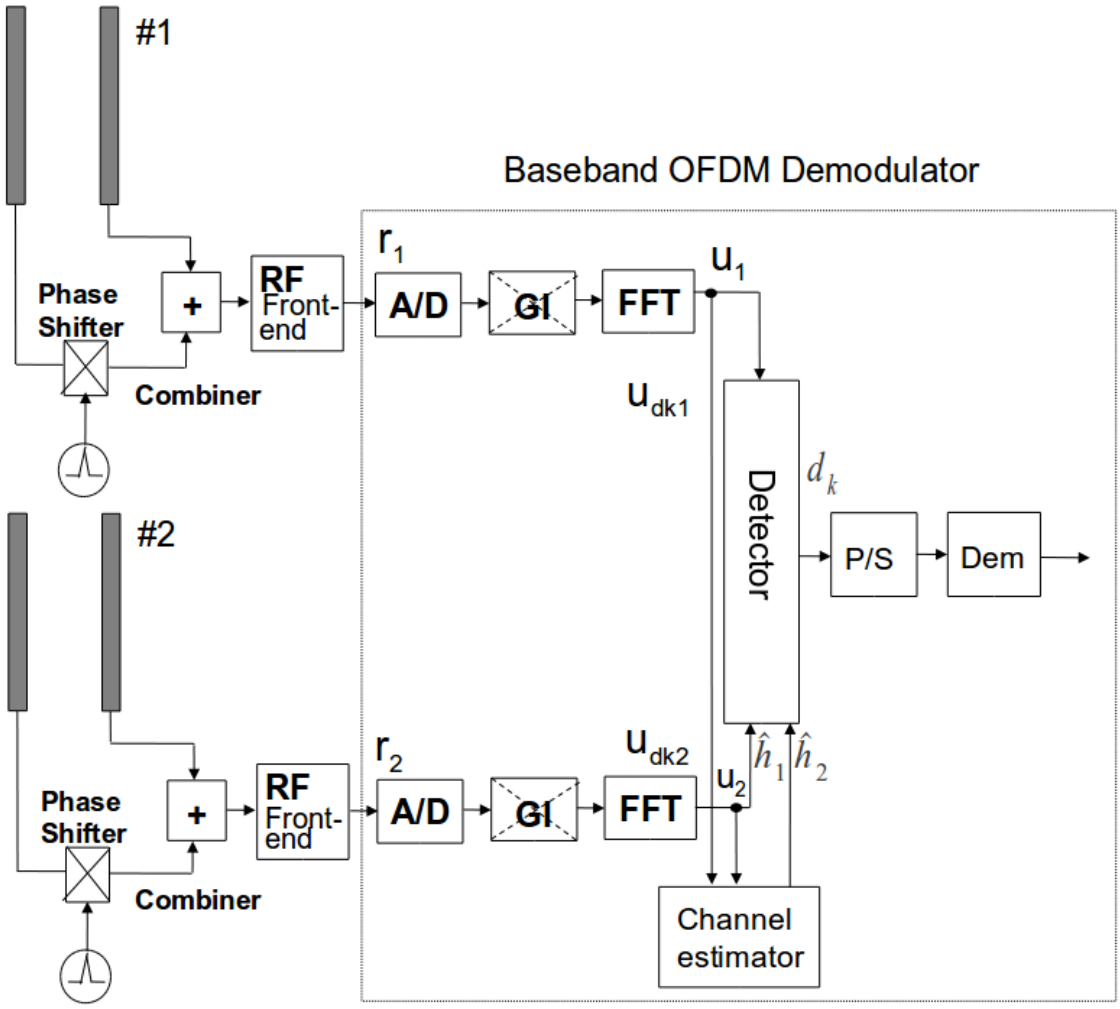

Figure 5.2. Block diagram of the MIMO-OFDM receiver with RF signal processing

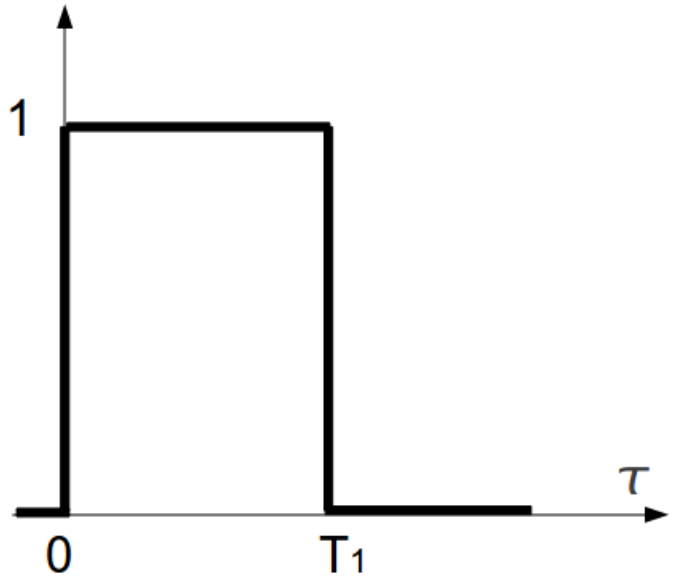

Figure 5.3. Rectangular shaping

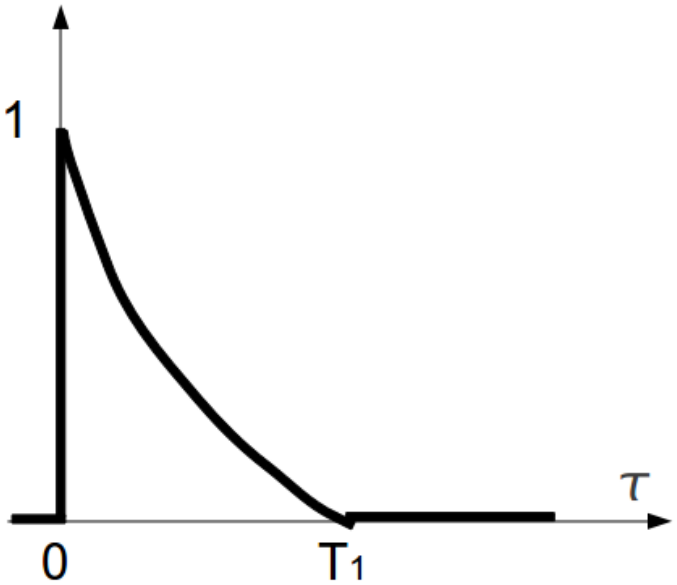

Figure 5.4. Exponential shaping

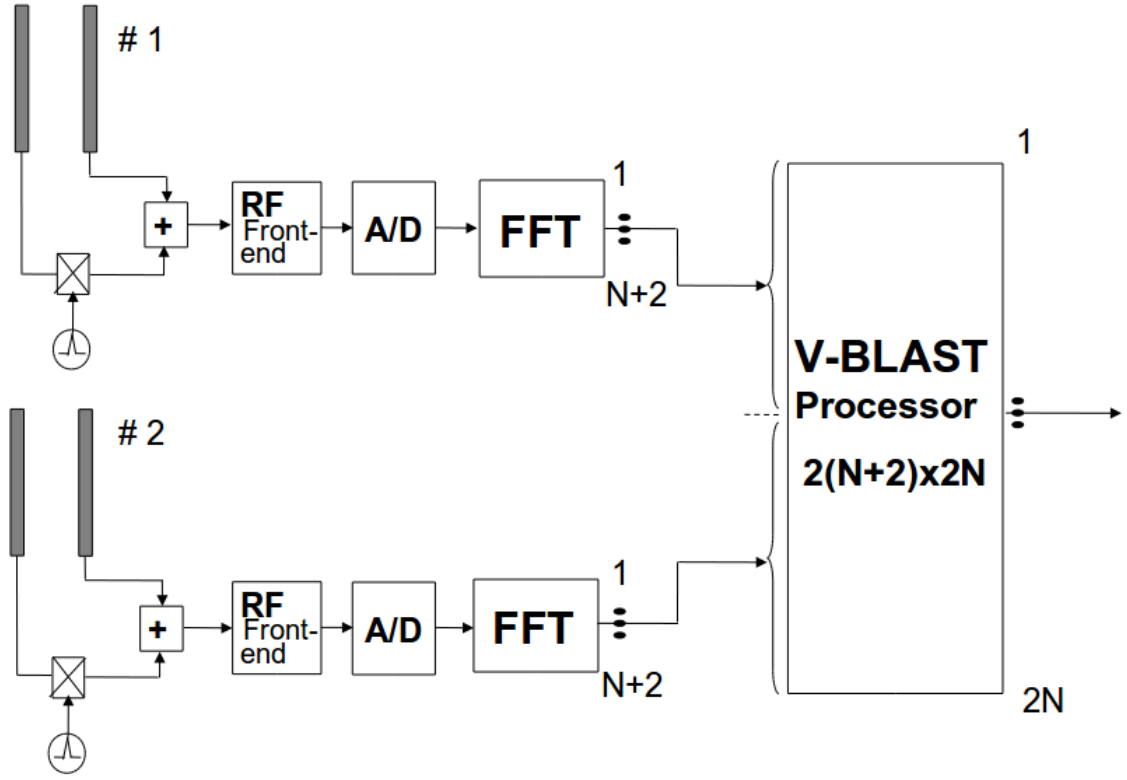

Figure 5.5. Block diagram of a MIMO decoder using 1 V-BLAST processor

$$\mathbf{H}_{i,j} = \begin{pmatrix} H_{1,-\frac{N}{2}} & 0 & \dots & \dots & \dots & \dots & \dots & \dots & \dots & 0 \\ H_{2,-\frac{N}{2}} & H_{1,-(\frac{N}{2}-1)} & 0 & \dots & \dots & \dots & \dots & \dots & \dots & \dots \\ 0 & H_{2,-(\frac{N}{2}-1)} & H_{1,-(\frac{N}{2}-2)} & 0 & \dots & \dots & \dots & \dots & \dots & \dots \\ \dots & 0 & H_{2,-(\frac{N}{2}-2)} & \ddots & 0 & \dots & \dots & \dots & \dots & \dots \\ \dots & \dots & 0 & \ddots & H_{1,-1} & 0 & \vdots & \vdots & \vdots & \vdots \\ \dots & \dots & \dots & 0 & H_{2,-1} & 0 & \dots & \dots & \dots & \dots \\ \dots & \dots & \dots & \dots & 0 & H_{1,+1} & 0 & \dots & \dots & \dots \\ \vdots & \vdots & \vdots & \vdots & 0 & H_{2,+1} & \ddots & 0 & \dots & \dots \\ \dots & \dots & \dots & \dots & \dots & 0 & \ddots & H_{1,+(\frac{N}{2}-2)} & 0 & \dots \\ \dots & \dots & \dots & \dots & \dots & \dots & 0 & H_{2,+(\frac{N}{2}-2)} & H_{1,+(\frac{N}{2}-1)} & 0 \\ \dots & \dots & \dots & \dots & \dots & \dots & \dots & 0 & H_{2,+(\frac{N}{2}-1)} & H_{1,+\frac{N}{2}} \\ 0 & \dots & \dots & \dots & \dots & \dots & \dots & \dots & 0 & H_{2,+\frac{N}{2}} \end{pmatrix} \tag{5.13}$$

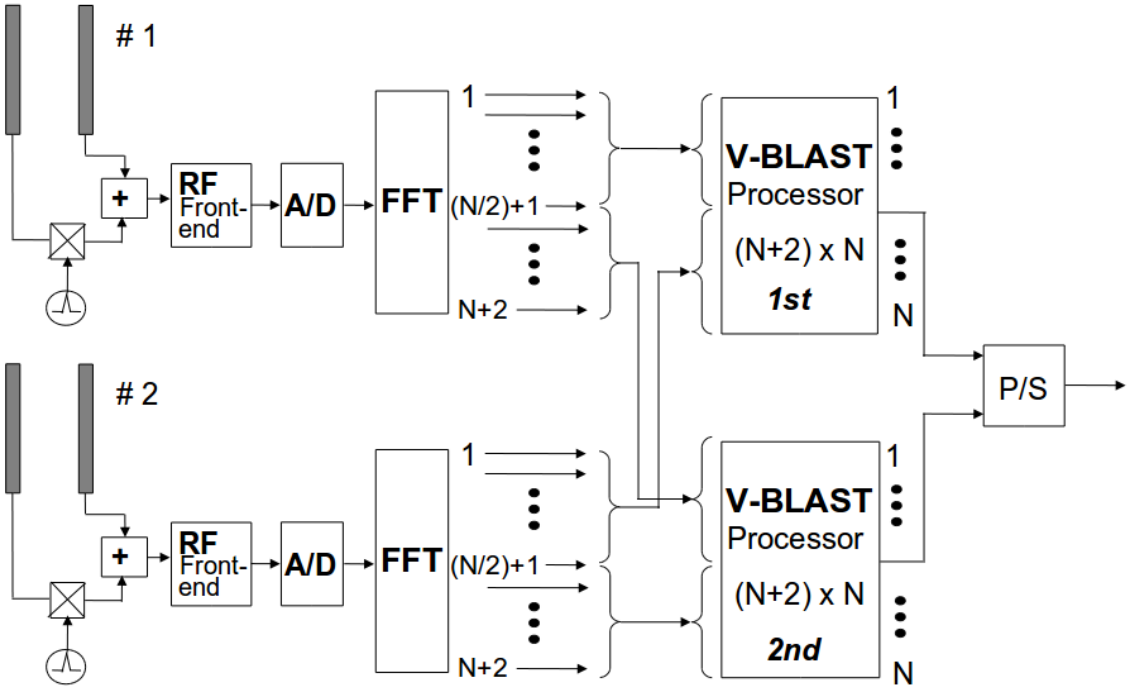

Figure 5.6. Block diagram of a MIMO decoder using 2 V-BLAST processors

$$\mathbf{H}_{up} = \begin{pmatrix} H_{1,-N/2} & 0 & \dots & 0 & H_{1,-N/2} & 0 & \dots & 0 \\ H_{2,-N/2} & \ddots & \ddots & \vdots & H_{2,-N/2} & \ddots & \ddots & \vdots \\ 0 & \ddots & \ddots & 0 & 0 & \ddots & \ddots & 0 \\ \vdots & \ddots & \ddots & H_{1,-1} & \vdots & \ddots & \ddots & H_{1,-1} \\ 0 & \dots & 0 & H_{2,-1} & 0 & \dots & 0 & H_{2,-1} \\ H_{1,-N/2} & 0 & \dots & 0 & H_{1,-N/2} & 0 & \dots & 0 \\ H_{2,-N/2} & \ddots & \ddots & \vdots & H_{2,-N/2} & \ddots & \ddots & \vdots \\ 0 & \ddots & \ddots & 0 & 0 & \ddots & \ddots & 0 \\ \vdots & \ddots & \ddots & H_{1,-1} & \vdots & \ddots & \ddots & H_{1,-1} \\ 0 & \dots & 0 & H_{2,-1} & 0 & \dots & 0 & H_{2,-1} \end{pmatrix}, \tag{5.15}$$

$$\mathbf{H}_{lo} = \begin{pmatrix} H_{1,+N/2} & 0 & \dots & 0 & H_{1,+N/2} & 0 & \dots & 0 \\ H_{2,+N/2} & \ddots & \ddots & \vdots & H_{2,+N/2} & \ddots & \ddots & \vdots \\ 0 & \ddots & \ddots & 0 & 0 & \ddots & \ddots & 0 \\ \vdots & \ddots & \ddots & H_{1,+1} & \vdots & \ddots & \ddots & H_{1,+1} \\ 0 & \dots & 0 & H_{2,+1} & 0 & \dots & 0 & H_{2,+1} \\ H_{1,+N/2} & 0 & \dots & 0 & H_{1,+N/2} & 0 & \dots & 0 \\ H_{2,+N/2} & \ddots & \ddots & \vdots & H_{2,+N/2} & \ddots & \ddots & \vdots \\ 0 & \ddots & \ddots & 0 & 0 & \ddots & \ddots & 0 \\ \vdots & \ddots & \ddots & H_{1,+1} & \vdots & \ddots & \ddots & H_{1,+1} \\ 0 & \dots & 0 & H_{2,+1} & 0 & \dots & 0 & H_{2,+1} \end{pmatrix} \tag{5.16}$$

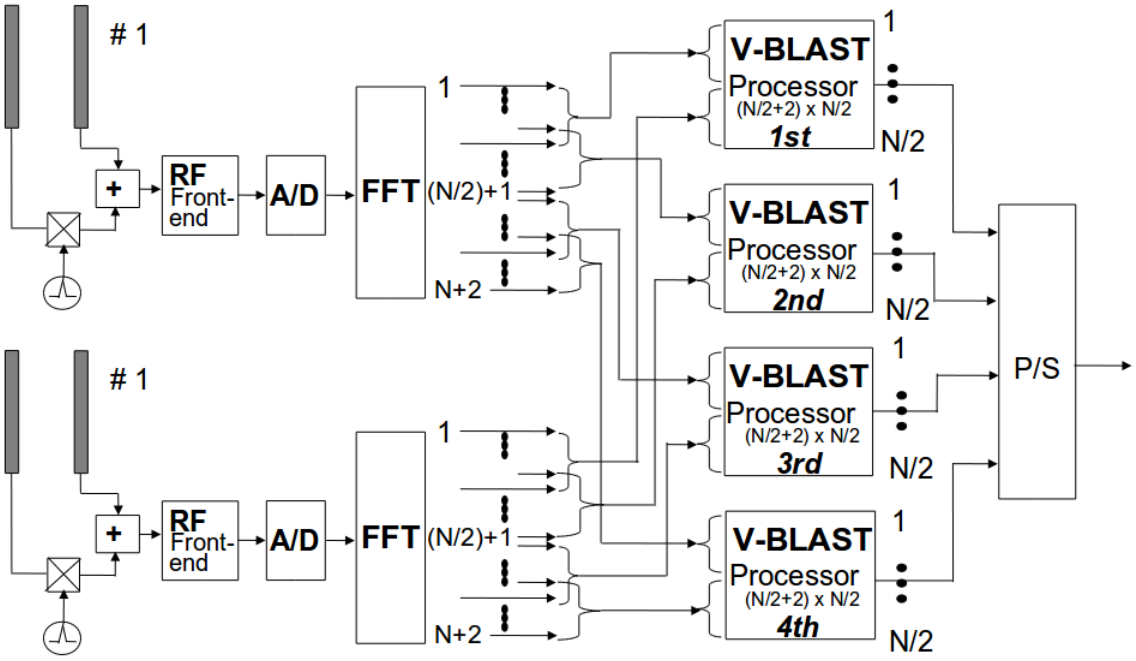

Figure 5.7. Block diagram of a MIMO decoder using 4 V-BLAST processors

$$\mathbf{H}_{uA} = \begin{pmatrix} H_{1,-N/2} & 0 & \dots & 0 & H_{1,-N/2} & 0 & \dots & 0 \\ H_{2,-N/2} & \ddots & \ddots & \vdots & H_{2,-N/2} & \ddots & \ddots & \vdots \\ 0 & \ddots & \ddots & 0 & 0 & \ddots & \ddots & 0 \\ \vdots & \ddots & \ddots & H_{1,-N/4} & \vdots & \ddots & \ddots & H_{1,-N/4} \\ 0 & \dots & 0 & H_{2,-N/4} & 0 & \dots & 0 & H_{2,-N/4} \\ H_{1,-N/2} & 0 & \dots & 0 & H_{1,-N/2} & 0 & \dots & 0 \\ H_{2,-N/2} & \ddots & \ddots & \vdots & H_{2,-N/2} & \ddots & \ddots & \vdots \\ 0 & \ddots & \ddots & 0 & 0 & \ddots & \ddots & 0 \\ \vdots & \ddots & \ddots & H_{1,-N/4} & \vdots & \ddots & \ddots & H_{1,-N/4} \\ 0 & \dots & 0 & H_{2,-N/4} & 0 & \dots & 0 & H_{2,-N/4} \end{pmatrix}, \tag{5.17}$$

$$\mathbf{H}_{uB} = \begin{pmatrix} H_{1,-N/4} & 0 & \dots & 0 & H_{1,-N/4} & 0 & \dots & 0 \\ H_{2,-N/4} & \ddots & \ddots & \vdots & H_{2,-N/4} & \ddots & \ddots & \vdots \\ 0 & \ddots & \ddots & 0 & 0 & \ddots & \ddots & 0 \\ \vdots & \ddots & \ddots & H_{1,-1} & \vdots & \ddots & \ddots & H_{1,-1} \\ 0 & \dots & 0 & H_{2,-1} & 0 & \dots & 0 & H_{2,-1} \\ H_{1,-N/4} & 0 & \dots & 0 & H_{1,-N/4} & 0 & \dots & 0 \\ H_{2,-N/4} & \ddots & \ddots & \vdots & H_{2,-N/4} & \ddots & \ddots & \vdots \\ 0 & \ddots & \ddots & 0 & 0 & \ddots & \ddots & 0 \\ \vdots & \ddots & \ddots & H_{1,-1} & \vdots & \ddots & \ddots & H_{1,-1} \\ 0 & \dots & 0 & H_{2,-1} & 0 & \dots & 0 & H_{2,-1} \end{pmatrix}, \tag{5.18}$$

$$\mathbf{H}_{lA} = \begin{pmatrix} H_{1,+N/2} & 0 & \dots & 0 & H_{1,+N/2} & 0 & \dots & 0 \\ H_{2,+N/2} & \ddots & \ddots & \vdots & H_{2,+N/2} & \ddots & \ddots & \vdots \\ 0 & \ddots & \ddots & 0 & 0 & \ddots & \ddots & 0 \\ \vdots & \ddots & \ddots & H_{1,+N/4} & \vdots & \ddots & \ddots & H_{1,N/4} \\ 0 & \dots & 0 & H_{2,+N/4} & 0 & \dots & 0 & H_{2,N/4} \\ H_{1,+N/2} & 0 & \dots & 0 & H_{1,+N/2} & 0 & \dots & 0 \\ H_{2,+N/2} & \ddots & \ddots & \vdots & H_{2,+N/2} & \ddots & \ddots & \vdots \\ 0 & \ddots & \ddots & 0 & 0 & \ddots & \ddots & 0 \\ \vdots & \ddots & \ddots & H_{1,+N/4} & \vdots & \ddots & \ddots & H_{1,+N/4} \\ 0 & \dots & 0 & H_{2,+N/4} & 0 & \dots & 0 & H_{2,+N/4} \end{pmatrix}, \tag{5.19}$$

$$\mathbf{H}_{IB} = \begin{pmatrix} H_{1,+N/4} & 0 & \dots & 0 & H_{1,+N/4} & 0 & \dots & 0 \\ H_{2,+N/4} & \ddots & \ddots & \vdots & H_{2,+N/4} & \ddots & \ddots & \vdots \\ 0 & \ddots & \ddots & 0 & 0 & \ddots & \ddots & 0 \\ \vdots & \ddots & \ddots & H_{1,+1} & \vdots & \ddots & \ddots & H_{1,+1} \\ 0 & \dots & 0 & H_{2,+1} & 0 & \dots & 0 & H_{2,+1} \\ H_{1,+N/4} & 0 & \dots & 0 & H_{1,+N/4} & 0 & \dots & 0 \\ H_{2,+N/4} & \ddots & \ddots & \vdots & H_{2,+N/4} & \ddots & \ddots & \vdots \\ 0 & \ddots & \ddots & 0 & 0 & \ddots & \ddots & 0 \\ \vdots & \ddots & \ddots & H_{1,+1} & \vdots & \ddots & \ddots & H_{1,+1} \\ 0 & \dots & 0 & H_{2,+1} & 0 & \dots & 0 & H_{2,+1} \end{pmatrix}, \tag{5.20}$$

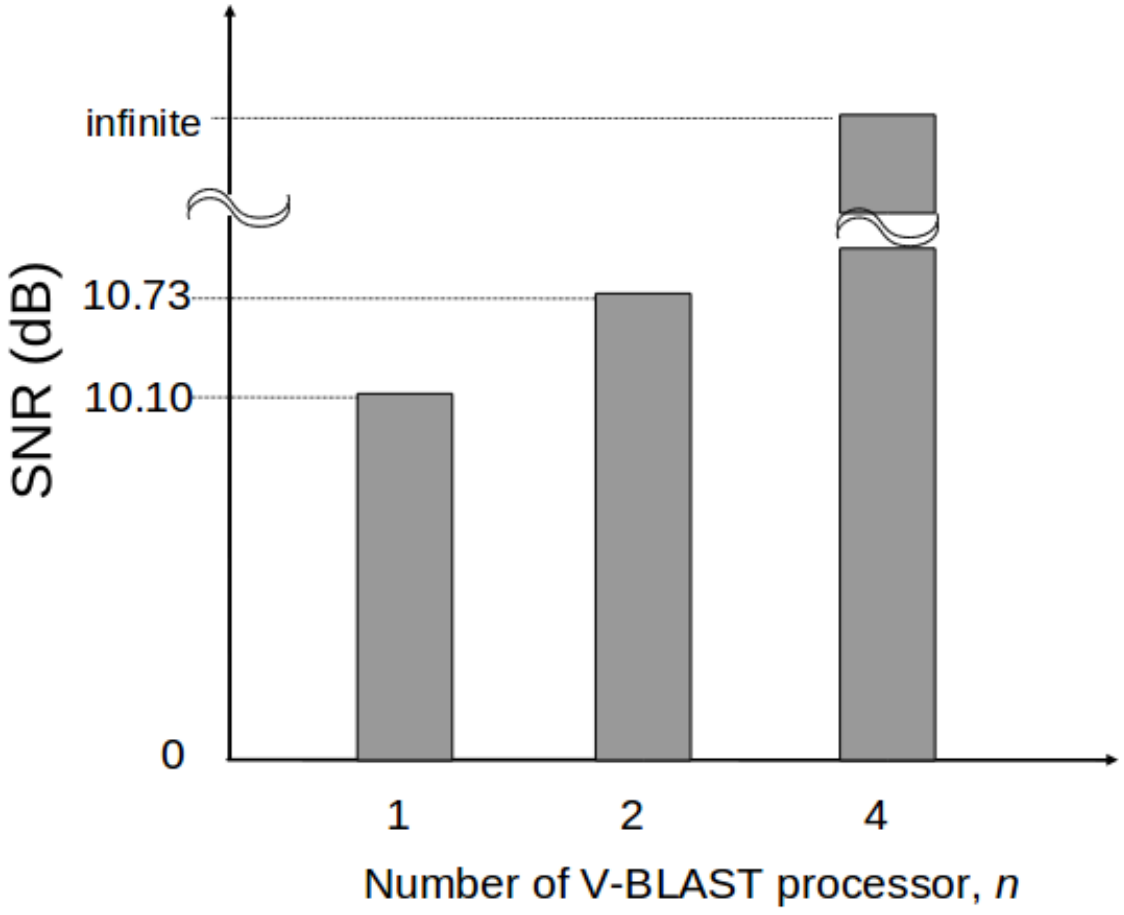

Figure 5.8. Error rate performances for n V-BLAST processors

Chapter 6

Simulation Results and Discussion

IN this section I will explain the simulation results and discussion.

6.1. System Parameter

The transmitted symbol belongs to a QPSK (Quadrature Phase Shift Keying) constellation and is obtained from the information bits through of usual modulation. A block diagram of the MIMO detection of the simulation is shown in Fig. 5.6. In this simulation the pilot sequence of HTLTF (High Throughput Long Training Field) based on IEEE 802.11n in 20 MHz frequency is used. This pilot sequence is given by Eq. (6.1).

$$\begin{aligned} \mathbf{HTLTF}_{28:28} = \{&1,1,1,1,1,1,1,1,1,1,1,1,1,1,1,1,1,1,1,1,1,1,1,1,1,1,1,1,1,1,1,1,\\ &1,1,1,1,1,1,1,0,1,1,1,1,1,1,1,1,1,1,1,1,1,1,1,1,1,1,1,1,1,1,1,1,\\ &1,1,1,1,1,1,1,1,1,1,1,1,1,1,1,1,1,1,1,1,1,1,1,1,1,1,1,1,1,1,1,1\} \end{aligned} \tag{6.1}$$

The total number of subcarriers is 56 and all simulation parameters are shown in Table 6.1. The multipath fading channel is generated by the Rayleigh fading channel model [13], IEEE 802.11n Typical Resident model channel (τ_s = 15 ns and B_c = 12.8 MHz) and Winner Channel Scenario A1 channel model (τ_s = 12.89 ns and B_c = 15.5 MHz), respectively. The Power Delay Profile (PDP) of the Winner channel model and IEEE 802.11n are shown in Tables 6.2 and 6.3 respectively.

Table 6.1. Simulation parameters

	Parameters	Value
Transmitter	Pilot Sequence	HTLTF
	Modulation	QPSK
	Number of sub-carriers	56
	FFT size	64
	Antenna Dimension	2x2
	Guard Interval Length (GI)	1/4
Channel	Rayleigh Fading	2-rays
	IEEE802.11n Typical Resident	9-path
	Winner Channel Scenario A1	12-path
Receiver	Channel Estimation	MMSE
	Equalization	V-BLAST

6.2. Performance Assessment

In this section, the results of computer simulation are shown for 2×2 MIMO-OFDM systems using RF signal processing over a two-rays Rayleigh fading channel model, IEEE 802.11n channel model and WINNER channel model. The *BER* characteristics of these three channel models are plotted in Figs. 6.2, 6.3 and 6.4. The performances are compared to conventional MIMO-OFDM systems for 2×4, 2×2, and SISO-OFDM system, respectively, using the same modulation schemes.

The technique to apply two-rays Rayleigh fading channel model can be explained as follows. The block diagram transceiver system using this channel model is shown in Fig.6.1. This figure explains that the channel impulse response (h) in the receiver antenna is the sum of impulse response in tranmitter antennas 1 and 2. The equation in time domain can be written by

$$h(\tau) = h_{00}\delta(\tau) + h_{01}\delta(\tau - T_d) + h_{10}\delta(\tau - T_{CSD}) + h_{11}\delta(\tau - T_d - T_{CSD}) \tag{6.2}$$

where $h_{\bullet,\bullet}$ denotes channel impulse coeficient in receiver from transmitter, T_d denotes time delay and T_{CSD} denotes cyclic shift. And the equation (6.2) can be rewritten in frequency domain as shown below

$$H(f) = h_{00} + h_{01}e^{-j2\pi fT_d} + h_{10}e^{-j2\pi fT_{CSD}} + h_{11}e^{-j2\pi f(T_d+T_{CSD})} \tag{6.3}$$

Table 6.2. Characteristics of IEEE802.11n typical resident 9-path channel model with τ_s = 15 ns and B_c = 12.8 MHz

Path	Power(dB)	Delay(ns)
1	0	0
2	-5.4287	10
3	-2.5162	20
4	-5.8905	30
5	-9.1603	40
6	-12.5105	50
7	-15.6126	60
8	-18.7147	70
9	-21.8168	80

In Fig. 6.2 we compare the *BER* of our approaches for several MIMO detectors. At $BER = 10^{-3}$ our proposed scheme gives improved performance with a diversity gain of 10.9 dB for an ideal channel and 9.45 dB for an estimated channel when compared to the conventional 2×2 MIMO-OFDM systems. Our proposed scheme also gives a diversity gain of 3.9 dB for an ideal channel and 2.55 dB for an estimated channel when compared to Maximum Likelihood Detection (MLD) (2×2).

Our scheme also gives a diversity gain over the IEEE 802.11n channel model and WINNER channel model as illustrated in Fig. 6.3 and Fig. 6.4. A MIMO-OFDM system using RF signal processing yields better results than conventional 2×2 MIMO-OFDM systems and SISO-OFDM systems.

Compared to the IEEE 802.11n channel model, our approach gives an improved performance at $BER = 10^{-2}$ with a diversity gain of 7.5 dB for an ideal channel and 5.5 dB for an estimated channel when compared to a 2×2 MIMO-OFDM system. In the case of the WINNER channel model, our approach gives an improved performance at $BER = 10^{-2}$ with a diversity gain of 7 dB for an ideal channel and 5 dB for an estimated channel when compared to conventional 2×2 MIMO-OFDM systems. Conventional 2×2 MIMO systems cannot give as much diversity gain as conventional 2×4 MIMO systems [14], but a 2×2 MIMO-OFDM using RF signal processing can yield better performance for increasing diversity gain than conventional 2×2 MIMO-OFDM

Table 6.3. Winner channel scenario A1 12-path channel model with τ_s = 12.89 ns and B_c = 15.5 MHz

Path	Power(dB)	Delay(ns)
1	0	0
2	-1.7	5
3	-6.2	10
4	-7.7	15
5	-9.3	20
6	-12.1	25
7	-12.7	30
8	-12.7	35
9	-14.7	45
10	-16.3	55
11	-16.8	65
12	-18.4	75

systems. MLD is an optimum detection algorithm and it provides the best transmission performance [15]. In the proposed scheme, in addition to the RF components at each receiver antenna, 2×2 scheme is also related to conventional 2×4 MIMO systems, our proposed scheme outperforms a 2×2 MIMO-OFDM using MLD in the conventional system.

6.3. Computational Cost

In this section the computational cost is discussed for MIMO decomposition for MIMO-OFDM using RF signal processing and conventional MIMO-OFDM system. The results of this evaluation are shown in Table 6.4 and Table 6.5. Bold font in these tables is for proposal. In these tables the computational complexity of our proposal (ZF, MMSE and V-BLAST for the first scheme) is higher than conventional (MLD). But the complexity of computational cost of proposed system (V-BLAST for second scheme) is comparable.

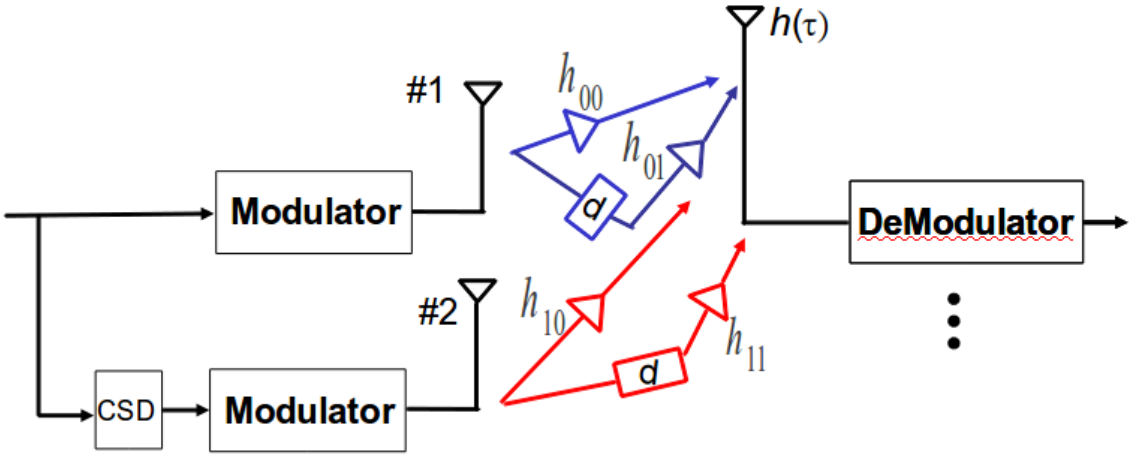

Figure 6.1. Block diagram of transceiver MIMO system using two-rays Rayleigh fading channel model

6.4. Performances Summary

In this section we show performances summary of the three model schemes for the three classification measurement.

The three model schemes are 2×2 V-BLAST, 2×4 V-BLAST and 2×2 RF-MIMO (proposed). The three classification are BER, computational cost and number of RF front-end. Performances summary for all schemes are shown in Table 6.6.

For the BER classification, 2×4 V-BLAST is the best, followed by 2×2 V-BLAST and 2 × 2 RF-MIMO (proposed). For the computational cost classification, 2 × 2 V-BLAST is the best, followed by 2 × 4 V-BLAST and RF-MIMO (proposed). And the other one, for the number of RF front-end classification, 2 × 2 RF-MIMO (proposed) and 2×2 V-BLAST are the best followed by 2×4 V-BLAST. Although the BER and the computational cost classification on 2 × 2 RF-MIMO (proposed) is lower than 2 × 4 V-BLAST, the 2×2 RF-MIMO (proposed) can reduce number of RF front-end. Reduction in the number of front-end will be followed by reducing power consumption. And the focus of our research is to reduce the number of RF front-ends.

Table 6.4. Computational cost for 4 QAM modulation

MIMO Detection	Multiplication	Addition
ZF (2x2)	$43.1x10^2$	$35.3x10^2$
MMSE (2x2)	$45.4x10^2$	$37.5x10^2$
MLD (2x2)	$23.8x10^3$	$20.0x10^3$
V-BLAST (2x2)	$11.0x10^3$	$79.0x10^2$
ZF (2x4)	$79.0x10^2$	$68.9x10^2$
MMSE (2x4)	$81.2x10^2$	$70.6x10^2$
V-BLAST (2x4)	$21.1x10^3$	$16.3x10^3$
Kalman (2x2)	$28.3x10^3$	$28.2x10^3$
ZF (2x2)	$11.8x10^6$	$11.7x10^6$
MMSE (2x2)	$11.8x10^6$	$11.7x10^6$
V-BLAST (2x2) -1	$23.5x10^6$	$23.4x10^6$
V-BLAST (2x2) -2	$59.7x10^5$	$59.1x10^5$

Table 6.5. Computational cost for 64 QAM modulation

MIMO Detection	Multiplication	Addition
ZF (2x2)	$43.1x10^2$	$35.3x10^2$
MMSE (2x2)	$45.4x10^2$	$37.5x10^2$
MLD (2x2)	$57.3x10^5$	$48.2x10^5$
V-BLAST (2x2)	$28.4x10^3$	$15.0x10^3$
ZF (2x4)	$79.0x10^2$	$68.9x10^2$
MMSE (2x4)	$81.2x10^2$	$70.6x10^2$
V-BLAST (2x4)	$38.6x10^3$	$23.5x10^3$
Kalman (2x2)	$28.3x10^3$	$28.2x10^3$
ZF (2x2)	$11.8x10^6$	$11.7x10^6$
MMSE (2x2)	$11.8x10^6$	$11.7x10^6$
V-BLAST (2x2) -1	$23.6x10^6$	$23.4x10^6$
V-BLAST (2x2) -2	$59.7x10^5$	$59.1x10^5$

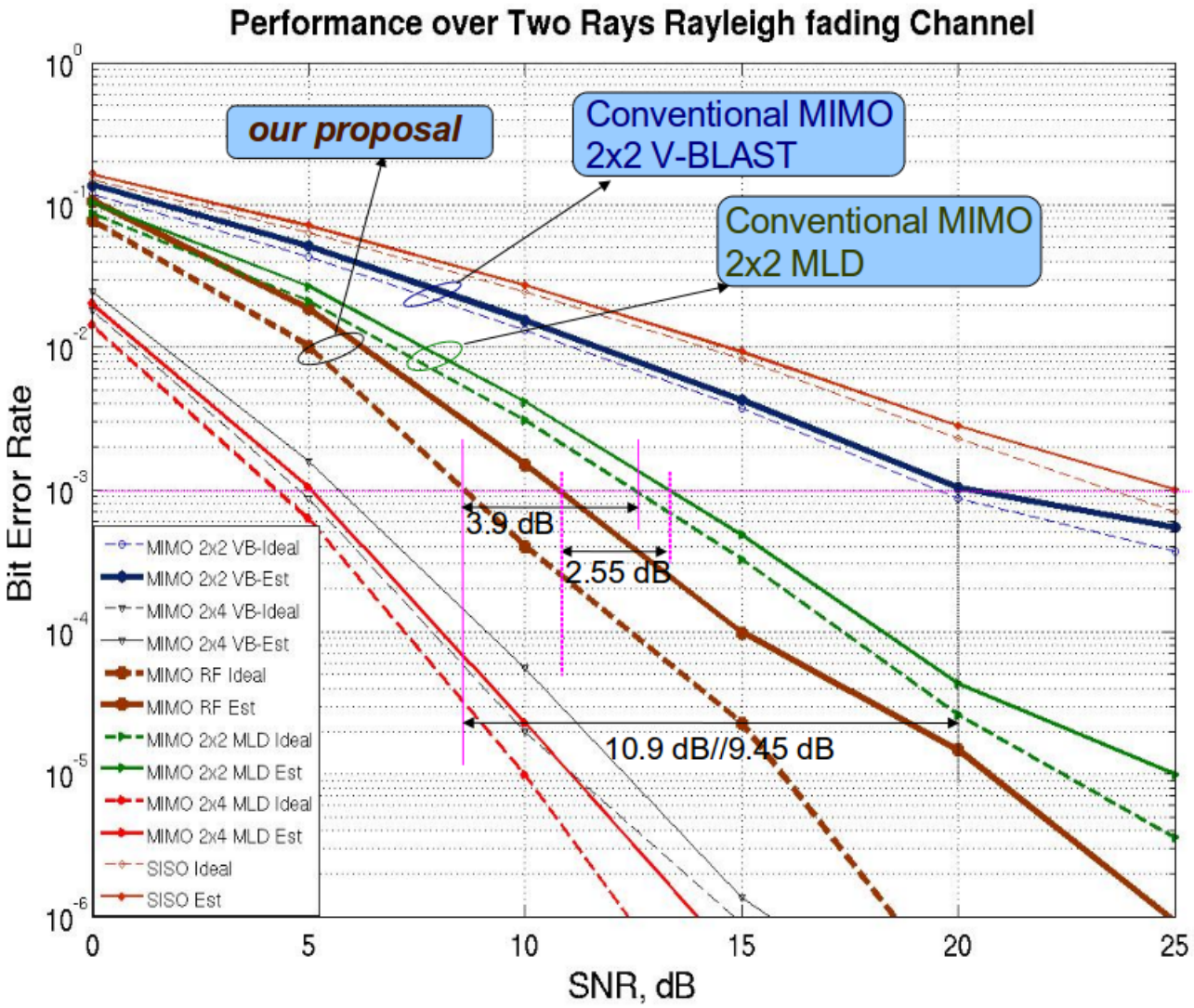

Figure 6.2. BER performance of MIMO-OFDM system using RF signal processing over two-rays Rayleigh fading channel model

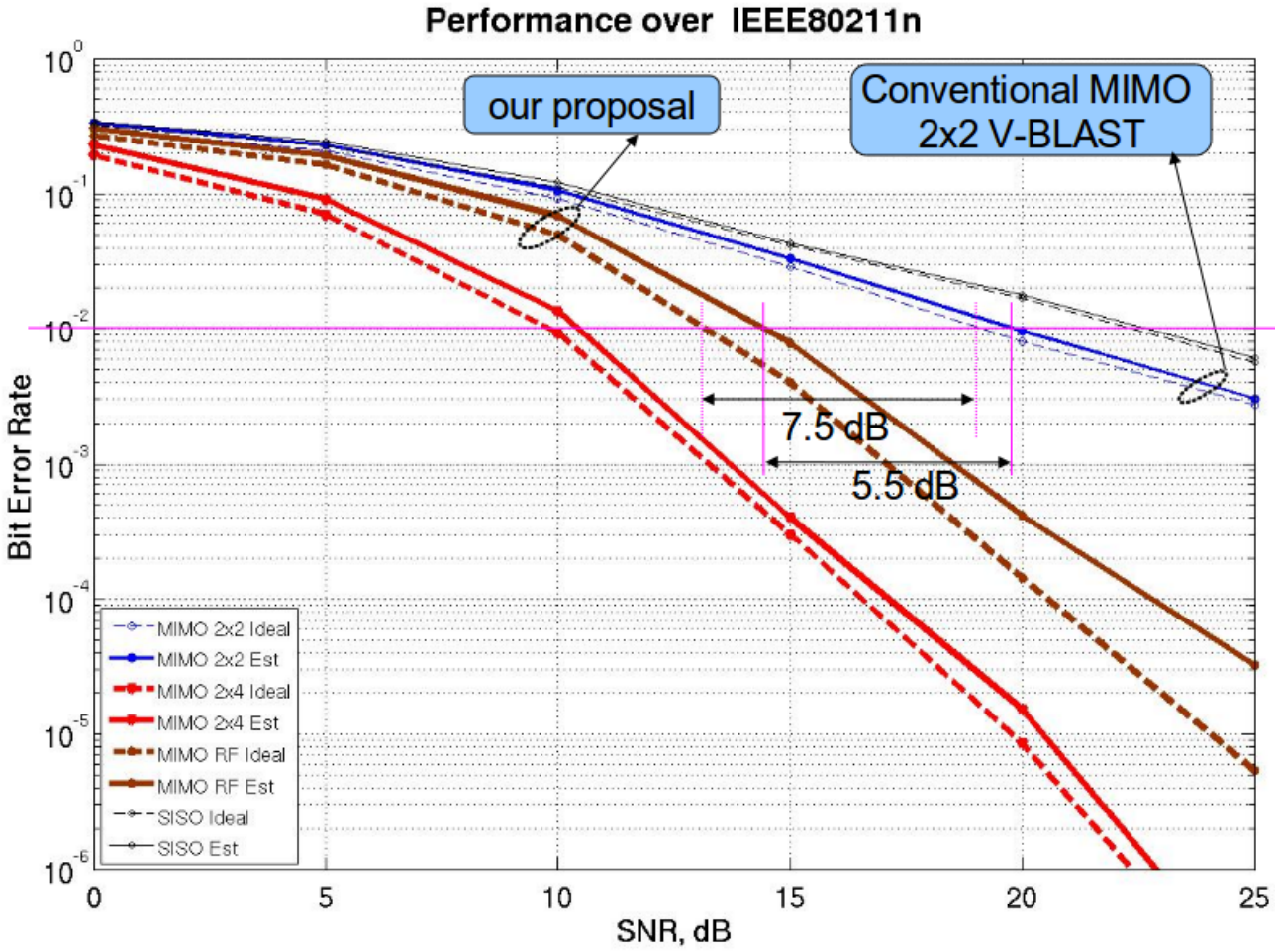

Figure 6.3. BER performance of MIMO-OFDM system using RF signal processing over IEEE 802.11n channel model

Table 6.6. Performances summary

Model Schemes	BER	Computational Cost	Number of RF front-end
2x2 V-BLAST	Bad	Best	2
2x4 V-BLAST	Best	Good	4
2x2 RF-MIMO (proposed)	Good	Bad	2

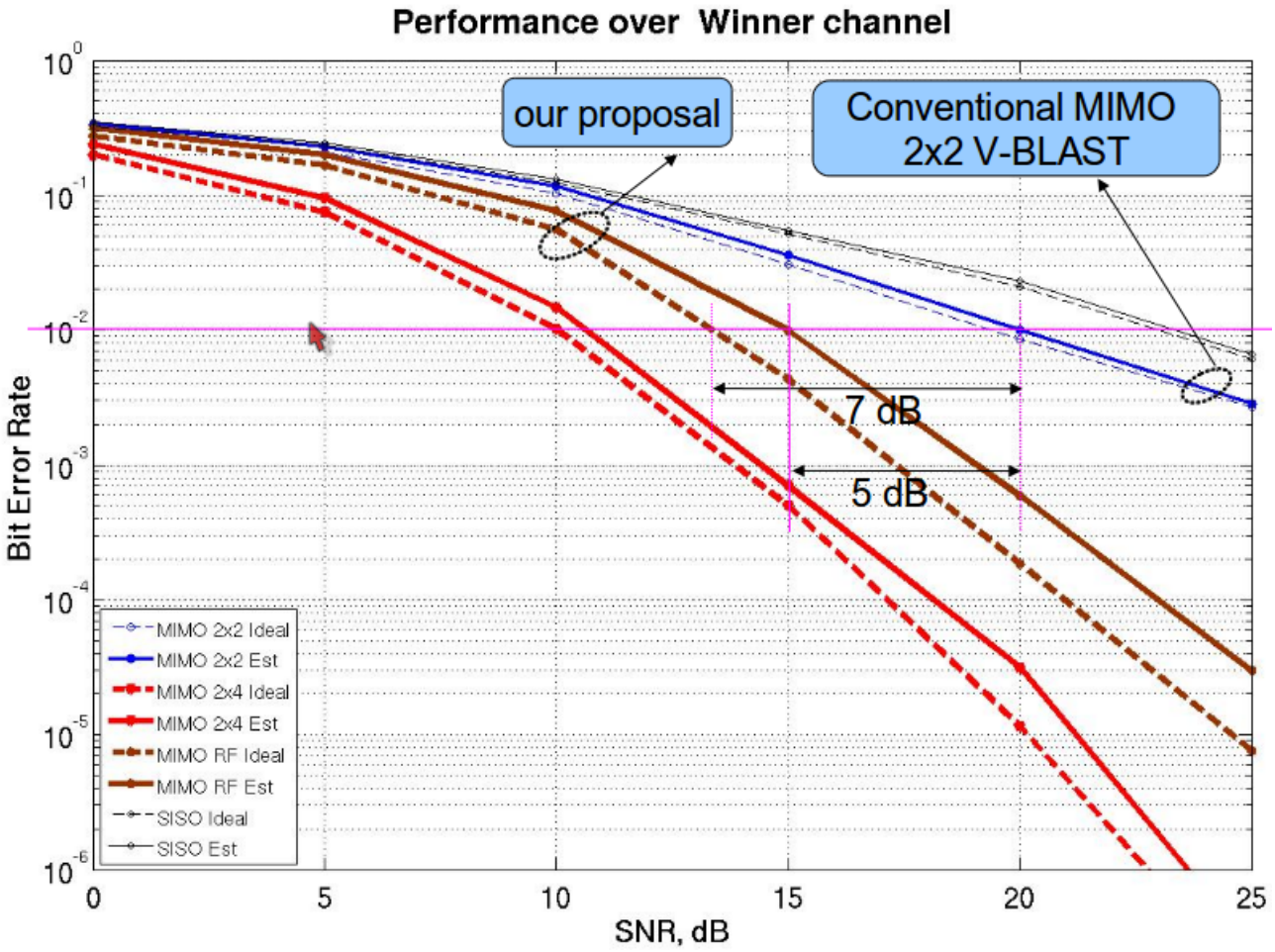

Figure 6.4. BER performance of MIMO-OFDM system using RF signal processing over Winner channel model

Chapter 7

Low Complexity MIMO Detection Using Kalman Filter

IN this section, let me introduced a Kalman filter-based MIMO decomposition algorithm in order to reduce the computational cost. The proposed scheme uses Kalman filter as a MIMO decomposition algorithm. Furthermore ECC (Error Corection Coding) is jointly used for improving the decomposition performance.

7.1. Kalman Filter

There are a lot of literatures to introduce Kalman filter algorithm such as [16] and [17]. In this section, Kalman filter addresses the general problem for trying to estimate the state $x \in \Re^n$ of a discrete-time controlled process that is given by Eq.(7.1) with an observation $z \in \Re^m$ shown in Eq.(7.2)

$$x_k = F x_{k-1} + v_{k-1} \tag{7.1}$$

$$z_k = H_k x_k + w_k \tag{7.2}$$

where F and H_k are known $n \times n$ dimensional state transition matrix and $m \times n$ dimension observation matrix, respectively. And v and w are mutually independent zero mean with Gaussian, with covariance matrices $\mathbf{Q}$ and $\mathbf{R}$, respectively.

The discrete Kalman filter algorithm is as follows:

Time Update (Predict) :
(A) Project the state ahead

$$\hat{x}_k = F\hat{x}_{k-1} \tag{7.3}$$

(B) Project the error covariance ahead

$$P_k = FP_{k-1}F^T + Q \tag{7.4}$$

Measurement Update(Correct) :
(A) Compute the Kalman Gain

$$K_k = P_k H^T (HP_k H^T + R)^{-1} \tag{7.5}$$

(B) Update the estimate with measurement z_k

$$\hat{x}_k = \hat{x}_k + K_k(z_k - H\hat{x}_k) \tag{7.6}$$

(C) Update the error covariance

$$P_k = (I - K_k H)P_{k-1} \tag{7.7}$$

7.2. Kalman Filter Based MIMO Detector

This section describes the proposed Kalman filter based MIMO detector. The proposed detector can reduce the computational cost required for the V-BLAST based MIMO detector shown in the last chapters. In general, Kalman filter works in time domain, but the concept of estimation techniques is in the same manner as in frequency domain processing. Therefore, we have proposed to estimate the number of symbols of subcarrier by considering the frequency shifting and frequency non-shifting. Let me start from SIMO (1×2) and then I extend it to MIMO (2×2).

7.2.1 Kalman Filter Based SIMO Detector (1×2)

Fig.7.3 shows the SIMO system (1×2) using four subcarriers for simplifying discussion. The signal forms are shown in Fig.7.5 for transmitter and in Fig.7.6 for receiver. The channel matrix for four subcarriers is shown in Eq.(7.8). The size of this matrix is

5×4, then it is converted to 1×2 size and as shown in Eq.(7.9). In case the number of subcarrier is four, the corresponding number of iteration in Kalman filter equalizer is $4 + 1 = 5$. So, the channnel matrices for this case are $H_1, \cdots, H_5$.

The output simulation for SIMO system using four subcarriers are shown in Fig.7.1 and Fig.7.2

$$H = \begin{pmatrix} h_{1,1} & 0 & 0 & 0 \\ h_{2,1} & h_{1,2} & 0 & 0 \\ 0 & h_{2,2} & h_{1,3} & 0 \\ 0 & 0 & h_{2,3} & h_{1,4} \\ 0 & 0 & 0 & h_{2,4} \end{pmatrix} \tag{7.8}$$

$$\begin{aligned} H_1 &= \begin{bmatrix} 0 & h_{1,1} \end{bmatrix} \\ H_2 &= \begin{bmatrix} h_{2,1} & h_{1,2} \end{bmatrix} \\ H_3 &= \begin{bmatrix} h_{2,2} & h_{1,3} \end{bmatrix} \\ H_4 &= \begin{bmatrix} h_{2,3} & h_{1,4} \end{bmatrix} \\ H_5 &= \begin{bmatrix} h_{2,4} & 0 \end{bmatrix} \end{aligned} \tag{7.9}$$

7.2.2 Kalman Filter Based 2×2 MIMO Detector

In Fig.7.4 shows SIMO system (2×2). To simplify the discussion I use four subcarriers. The signal forms at transmitter and receiver look like similar as in SIMO system. The channel matrix for four subcarrier are shown in Eq. (7.10). The size of this matrix is 10×8, then it is converted to 2×4 size as shown in Eq.(7.11). In case the number of subcarrier is four, the corresponding number of iteration in Kalman filter equalizer is $4 + 1 = 5$. So, the channnel matrices for this case are $H_1, \cdots, H_5$.

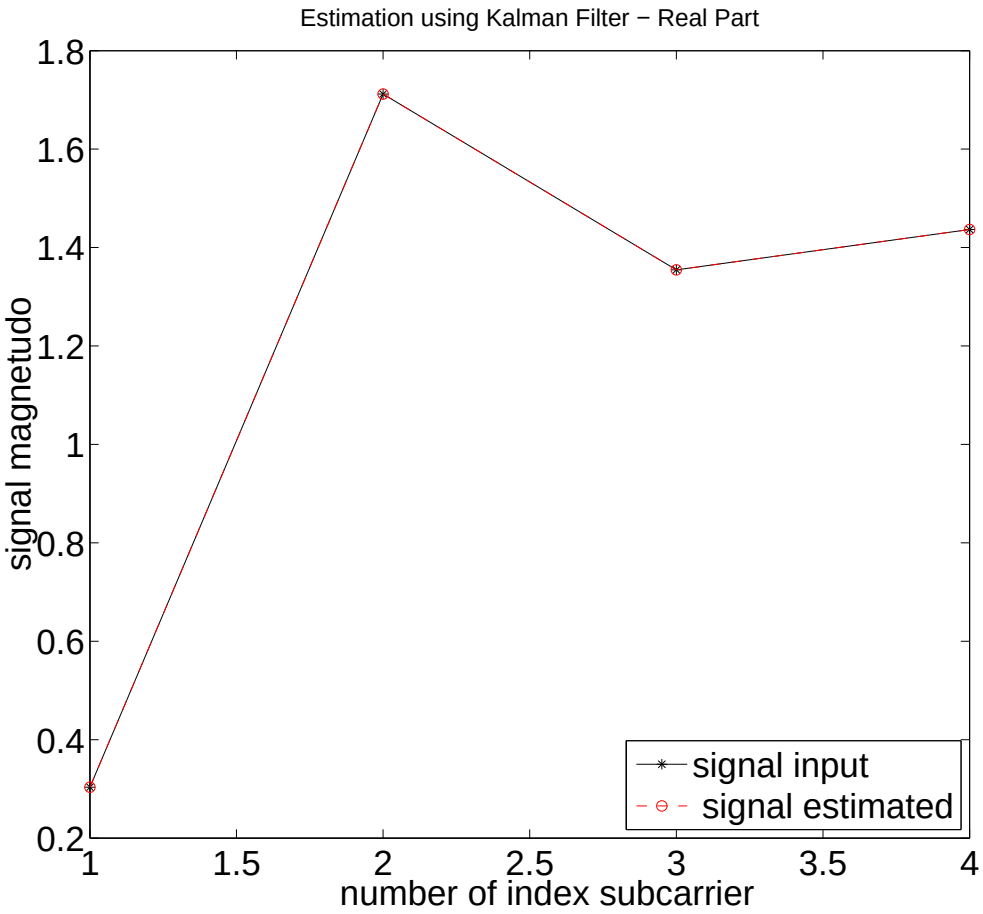

Figure 7.1. Kalman filter equalizer in SIMO system in real part

$$H = \begin{pmatrix} h_{1,1} & 0 & 0 & 0 & h_{1,1} & 0 & 0 & 0 \\ h_{2,1} & h_{1,2} & 0 & 0 & h_{2,1} & h_{1,2} & 0 & 0 \\ 0 & h_{2,2} & h_{1,3} & 0 & 0 & h_{2,2} & h_{1,3} & 0 \\ 0 & 0 & h_{2,3} & h_{1,4} & 0 & 0 & h_{2,3} & h_{1,4} \\ 0 & 0 & 0 & h_{2,4} & 0 & 0 & 0 & h_{2,4} \\ h_{1,1} & 0 & 0 & 0 & h_{1,1} & 0 & 0 & 0 \\ h_{2,1} & h_{1,2} & 0 & 0 & h_{2,1} & h_{1,2} & 0 & 0 \\ 0 & h_{2,2} & h_{1,3} & 0 & 0 & h_{2,2} & h_{1,3} & 0 \\ 0 & 0 & h_{2,3} & h_{1,4} & 0 & 0 & h_{2,3} & h_{1,4} \\ 0 & 0 & 0 & h_{2,4} & 0 & 0 & 0 & h_{2,4} \end{pmatrix} \tag{7.10}$$

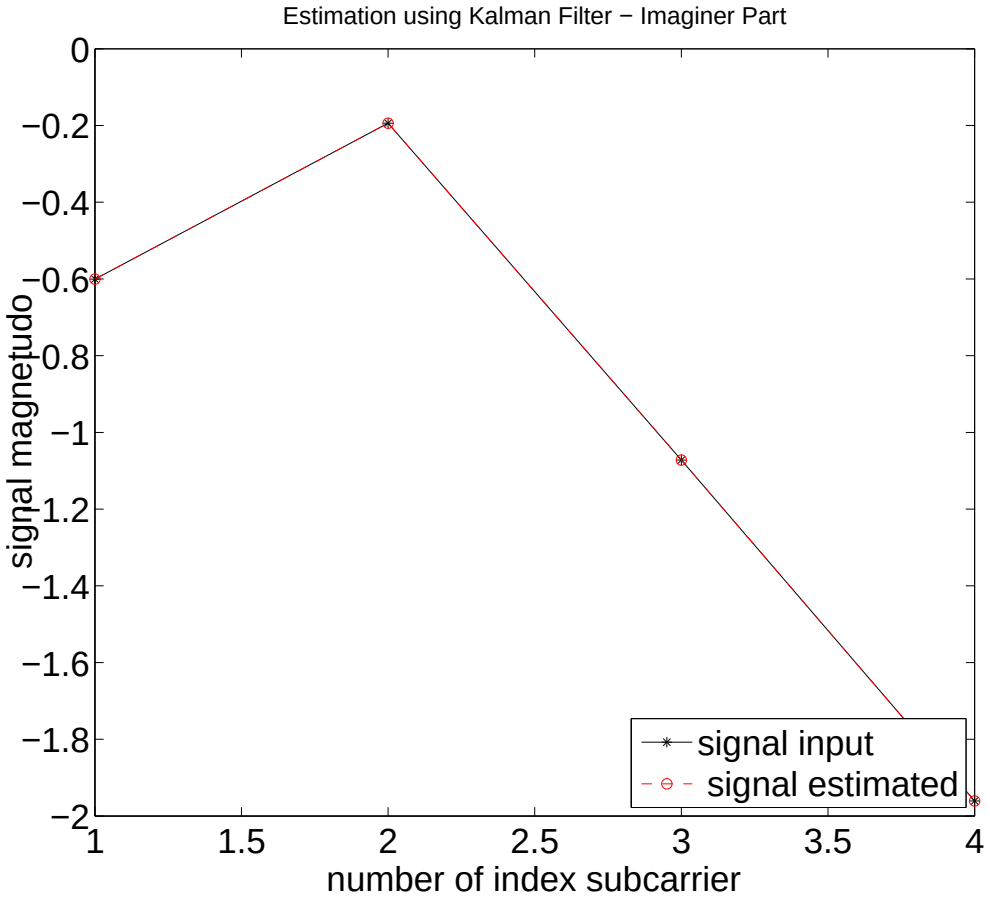

Figure 7.2. Kalman filter equalizer in SIMO system in imaginer part

$$
\begin{aligned}
H_1 &= \begin{bmatrix} 0 & h_{1,1} & 0 & h_{1,1} \\ 0 & h_{1,1} & 0 & h_{1,1} \end{bmatrix} \\
H_2 &= \begin{bmatrix} h_{2,1} & h_{1,2} & h_{2,1} & h_{1,2} \\ h_{2,1} & h_{1,2} & h_{2,1} & h_{1,2} \end{bmatrix} \\
H_3 &= \begin{bmatrix} h_{2,2} & h_{1,3} & h_{2,2} & h_{1,3} \\ h_{2,2} & h_{1,3} & h_{2,2} & h_{1,3} \end{bmatrix} \\
H_4 &= \begin{bmatrix} h_{2,3} & h_{1,4} & h_{2,3} & h_{1,4} \\ h_{2,3} & h_{1,4} & h_{2,3} & h_{1,4} \end{bmatrix} \\
H_5 &= \begin{bmatrix} h_{2,4} & 0 & h_{2,4} & 0 \\ h_{2,4} & 0 & h_{2,4} & 0 \end{bmatrix}
\end{aligned} \tag{7.11}
$$

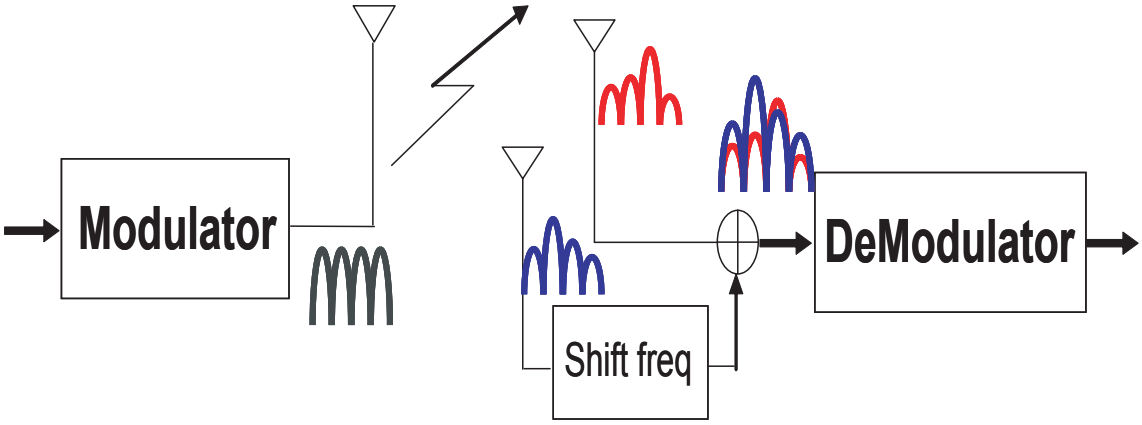

Figure 7.3. SIMO system

The output simulation for MIMO system using four subcarriers as shown in Fig.7.7, Fig.7.8, Fig.7.9 and Fig.7.10.

7.2.3 Kalman Filter Based MIMO Detector with RF signal processing

In this section I apply Kalman filter for MIMO detector with RF signal processing. The channel matrix size is 116×112, and I convert it to chanel matrices of size 2×4. Then I have 58 channel matrices of size 2×4 as shown in Eq.7.12. Based on IEEE80211n WLAN standard, the pilot signal has a DC signal and the signal form is shown in Fig.7.11.

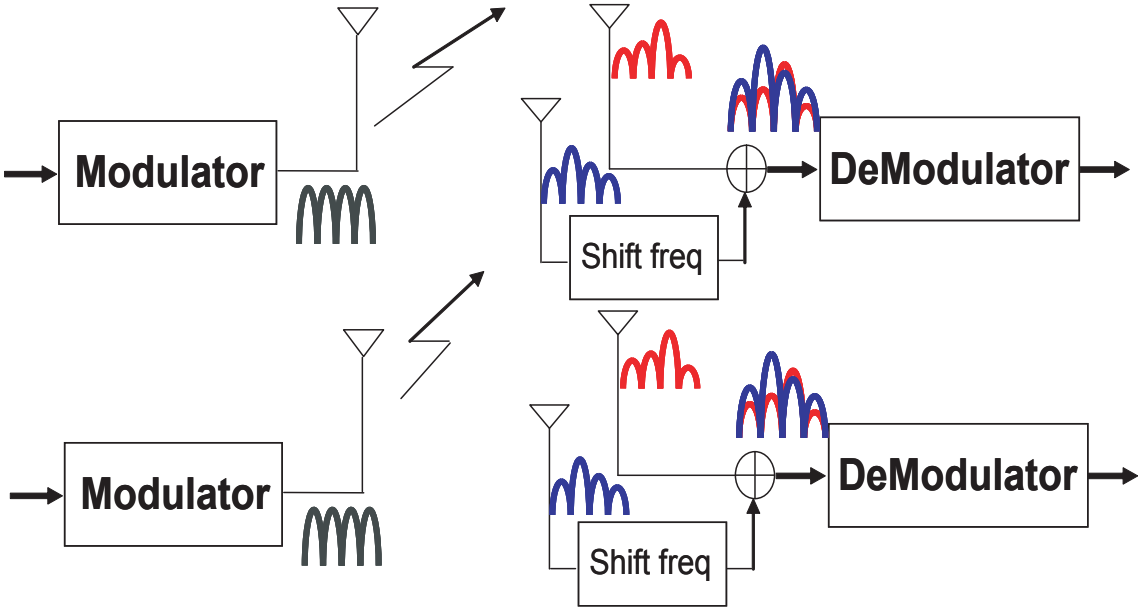

Figure 7.4. MIMO system

$$
\begin{aligned}
H_1 &= \begin{bmatrix} 0 & h_{1,1} & 0 & h_{1,1} \\ 0 & h_{1,1} & 0 & h_{1,1} \end{bmatrix} \\
H_2 \cdots H_{28} &= \begin{bmatrix} h_{2,1} & h_{1,2} & h_{2,1} & h_{1,2} \\ h_{2,1} & h_{1,2} & h_{2,1} & h_{1,2} \end{bmatrix} \\
H_{29} &= \begin{bmatrix} h_{2,29} & 0 & h_{2,29} & 0 \\ h_{2,29} & 0 & h_{2,29} & 0 \end{bmatrix} \\
H_{30} &= \begin{bmatrix} 0 & h_{1,30} & 0 & h_{1,30} \\ 0 & h_{1,30} & 0 & h_{1,30} \end{bmatrix} \\
H_{31} \cdots H_{57} &= \begin{bmatrix} h_{2,31} & h_{1,32} & h_{2,31} & h_{1,32} \\ h_{2,31} & h_{1,32} & h_{2,31} & h_{1,32} \end{bmatrix} \\
H_{58} &= \begin{bmatrix} h_{2,58} & 0 & h_{2,58} & 0 \\ h_{2,58} & 0 & h_{2,58} & 0 \end{bmatrix}
\end{aligned} \tag{7.12}
$$

In Eq.7.2 I have components of equation as in Eq.7.13 for z_k, Eq.7.14 for channel

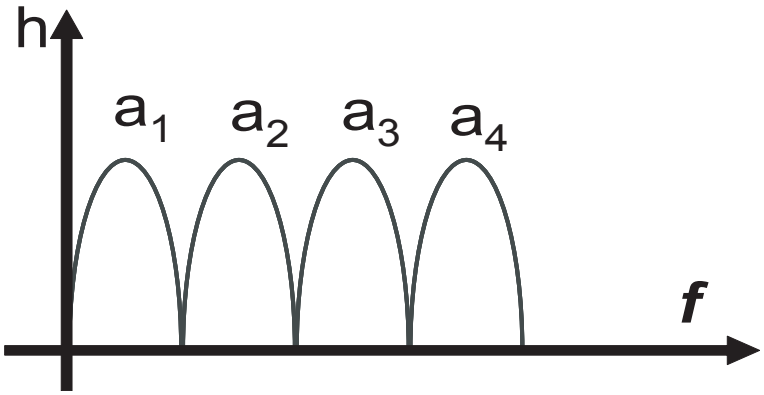

Figure 7.5. Signal four subcarriers in transmitter SIMO system

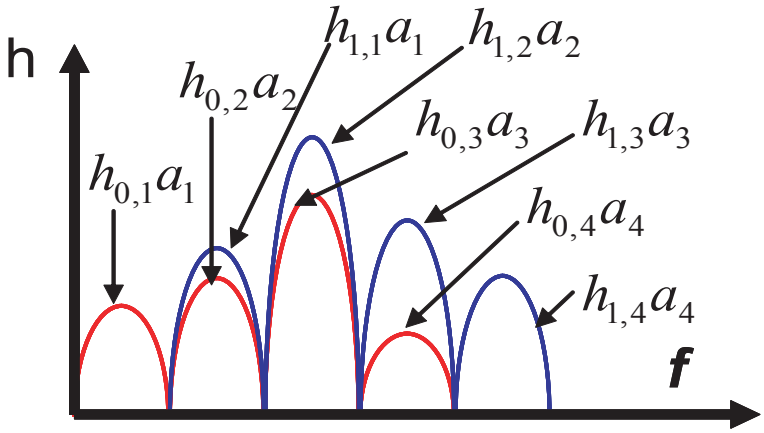

Figure 7.6. Signal four subcarriers in receiver SIMO system

matrices and Eq.7.15 for input state, and k refers to k-th carrier number.

$$z_k = \begin{pmatrix} z_k^{(0)} \\ z_k^{(1)} \end{pmatrix} \tag{7.13}$$

$$H_k = \begin{pmatrix} h_{k,k-1} & h_{k,k} & h_{k,k-1} & h_{k,k} \\ h_{k,k-1} & h_{k,k} & h_{k,k-1} & h_{k,k} \end{pmatrix} \tag{7.14}$$

$$x = \begin{pmatrix} x_{k-1}^{(0)} \\ x_k^{(0)} \\ x_{k-1}^{(1)} \\ x_k^{(1)} \end{pmatrix} \tag{7.15}$$

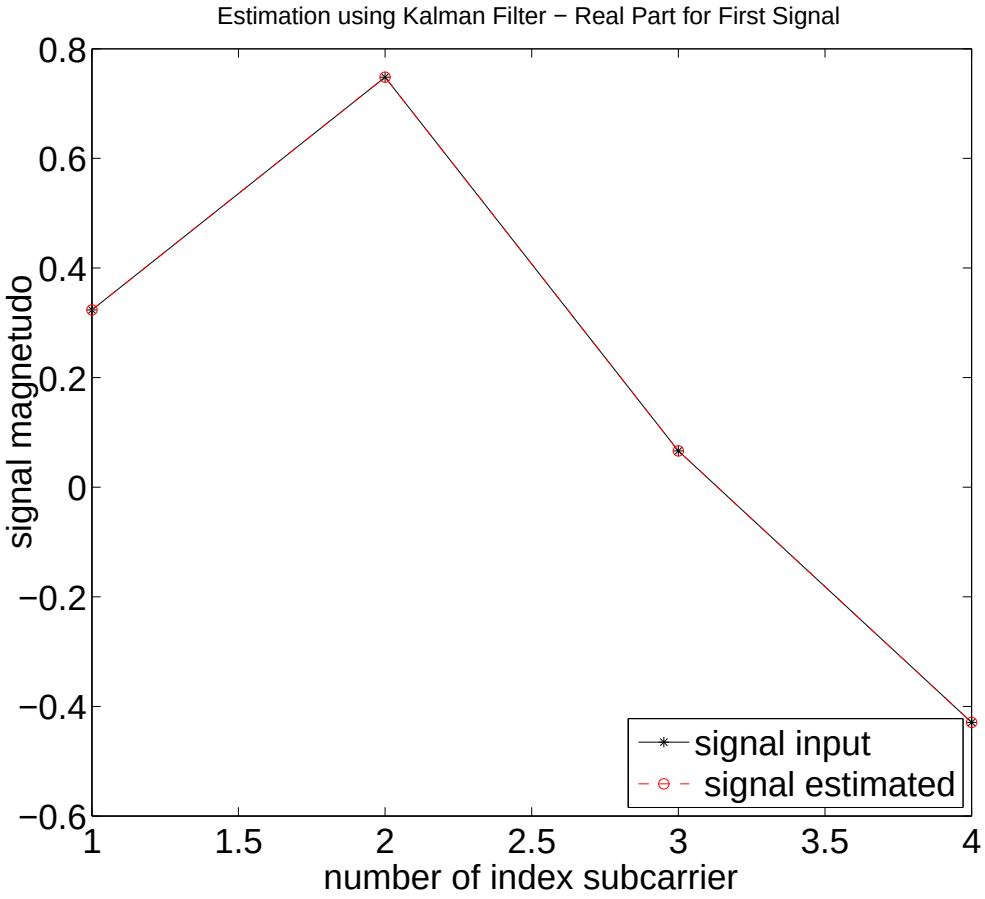

Figure 7.7. Kalman filter equalizer in MIMO system in real part for first signal

The state matrices of F is shown in Eq.(7.16)

$$F = \begin{pmatrix} 0 & 1 & 0 & 0 \\ 0 & 0 & 0 & 0 \\ 0 & 0 & 0 & 1 \\ 0 & 0 & 0 & 0 \end{pmatrix} \tag{7.16}$$

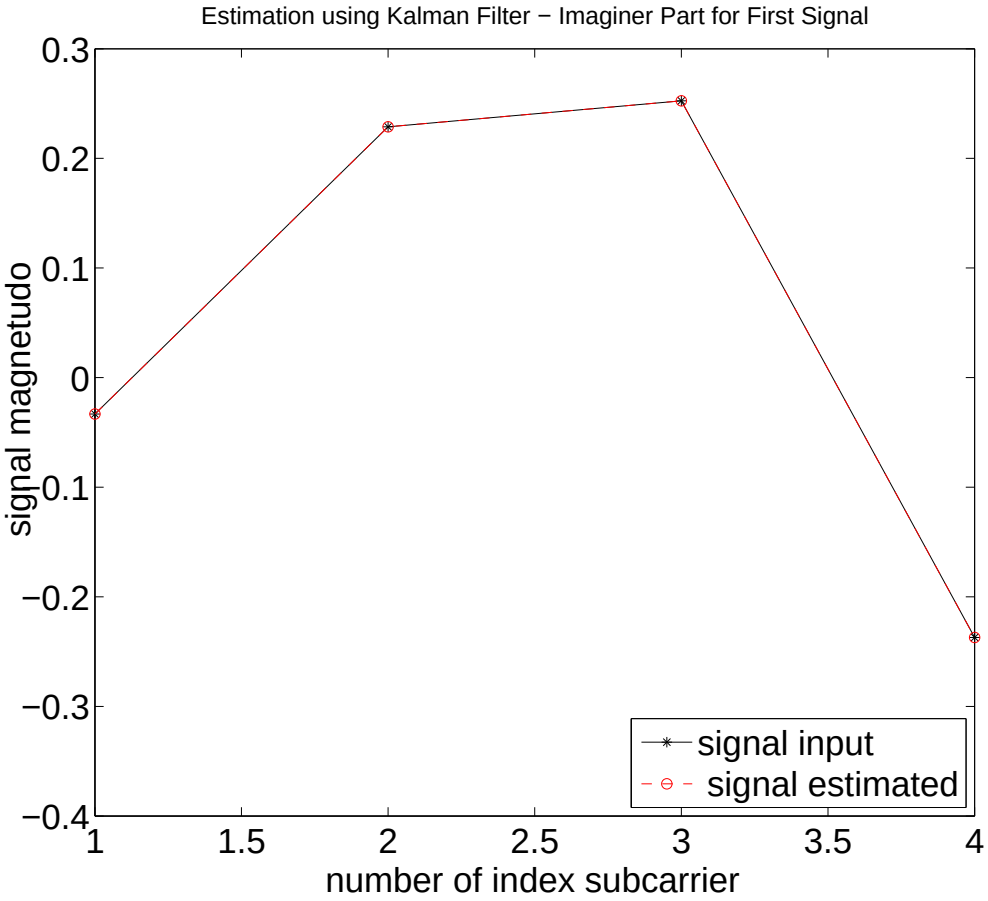

Figure 7.8. Kalman filter equalizer in MIMO system in imaginer part for first signal

7.3. Performance of the RF signal-processing Based Diversity Scheme for Coded MIMO-OFDM Systems

In this section I evaluate the bit error rate performance with error correction coding (ECC) techniques. The block diagrams of coded transmitter and coded receiver are shown in Fig.7.12 and in Fig.7.13, respectively. In the encoder I use convolutional coding with coding rate = $1/2$ and constraint length is 7 and the generator is [131 171]. And for decoding I use Viterbi decoding.

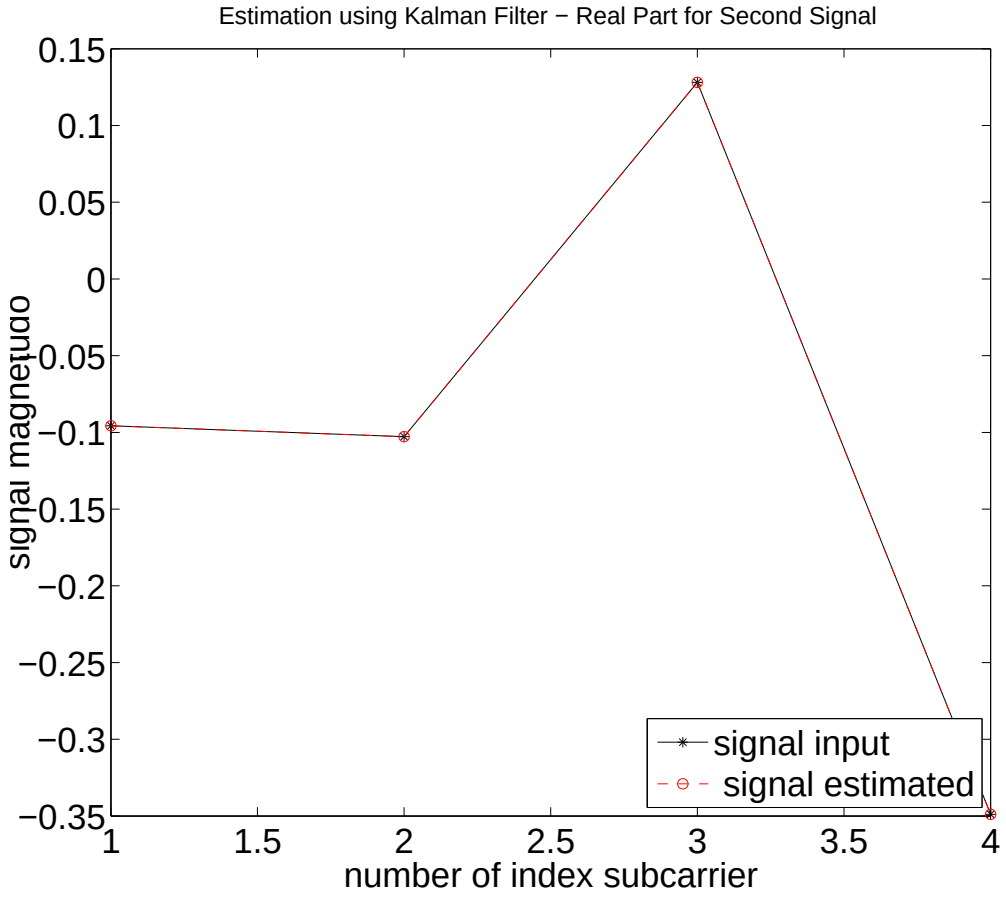

Figure 7.9. Kalman filter equalizer in MIMO system in real part for second signal

7.4. Performance Assessment

The results of the simulation for a 2 x 2 MIMO-OFDM system using RF signal processing over a two-rays Rayleigh fading channel model are shown in this section. The BER characteristics are plotted in Figs. 7.14 and 7.15. The performances are compared to four methods, those are (a) traditional MIMO-OFDM system using MLD detector, (b) RF signal-processing-based diversity scheme for uncoded MIMO-OFDM using V-BLAST detector [13], (c) RF signal-processing-based diversity scheme for coded MIMO-OFDM using MMSE detector and (d) Kalman filter detector using the same modulation schemes. In these figures the BER of our approaches is compared for

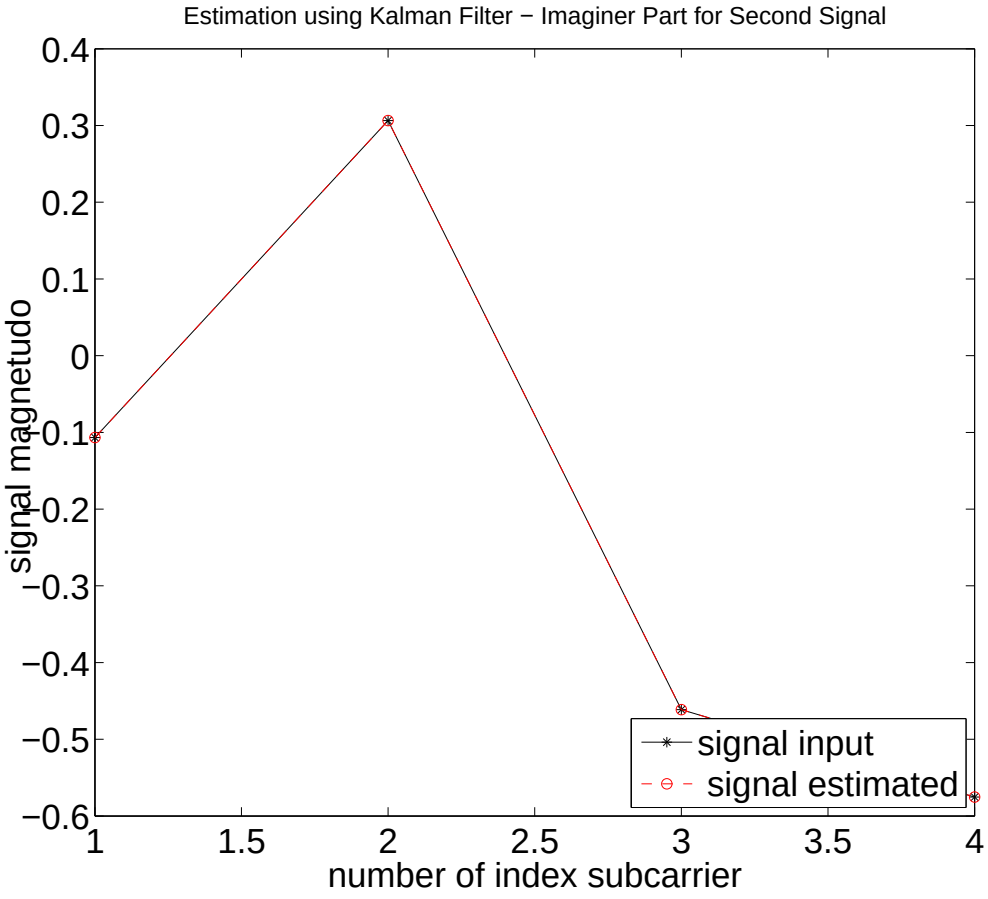

Figure 7.10. Kalman filter equalizer in MIMO system in imaginer part for second signal

various kinds of MIMO detector for both ideal and estimated channels. For Kalman filter based MIMO detector with the error corection coding (ECC) technique, shows that our approach has improved performance compared to a MLD detector for the rank of SNR from 0 through 5 dB and to a V-BLAST detector for 0 until 16 dB SNR for an ideal channel (Fig.7.14). Our proposal also has improved performance to a MLD detector for 0 until 6 dB and to a V-BLAST detector for 0 until 21 dB SNR for an estimated channel (Fig. 7.15). Comparison with MMSE detector, the performance of Kalman filter approach is still low.

The approach of Kalman filter based MIMO detector has disadvantage that it can-

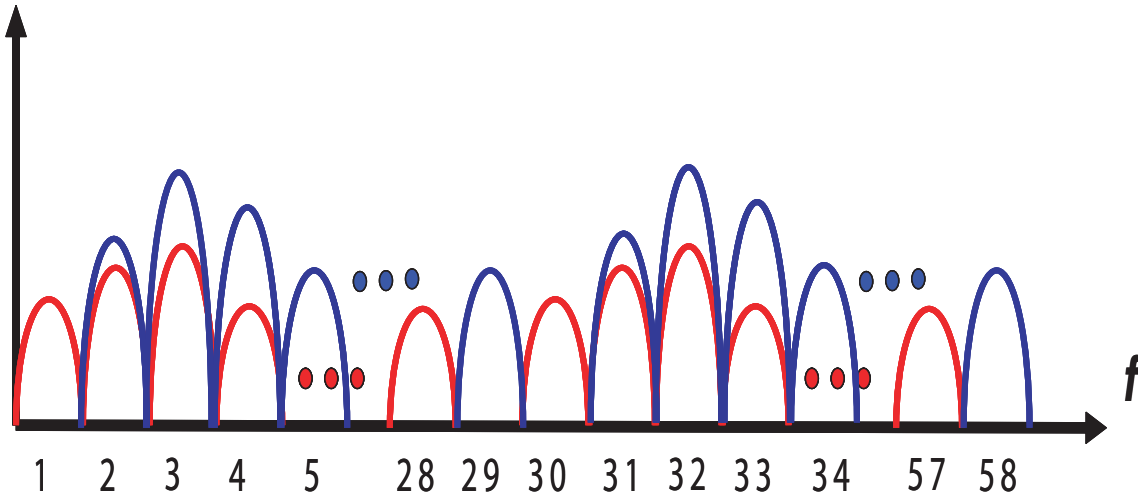

Figure 7.11. Signal 56 subcarriers in receiver MIMO system

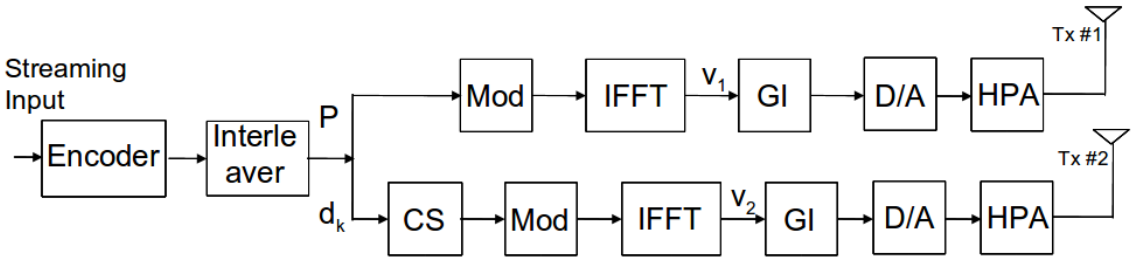

Figure 7.12. Block diagram of coded MIMO-OFDM RF signal-processing transmitter

not be equalized properly of the symbol for the existing measurement noise covariance (R) (the variance around $0.0562 \sim 1$) . The Kalman filter works well if the variance is very small. It is difficult/ impossible to get it, since the most common minimum variance is approximately 0.0562 (SNR = 25 dB).

However, in the MMSE detector, all existing variance can be processed properly. That is the reason why the Kalman filter based MIMO detector in our scheme is lower performance than MMSE. Then the Kalman filter based detector can reduce the complexity of computational cost compared with several detectors as shown in Table 7.1.

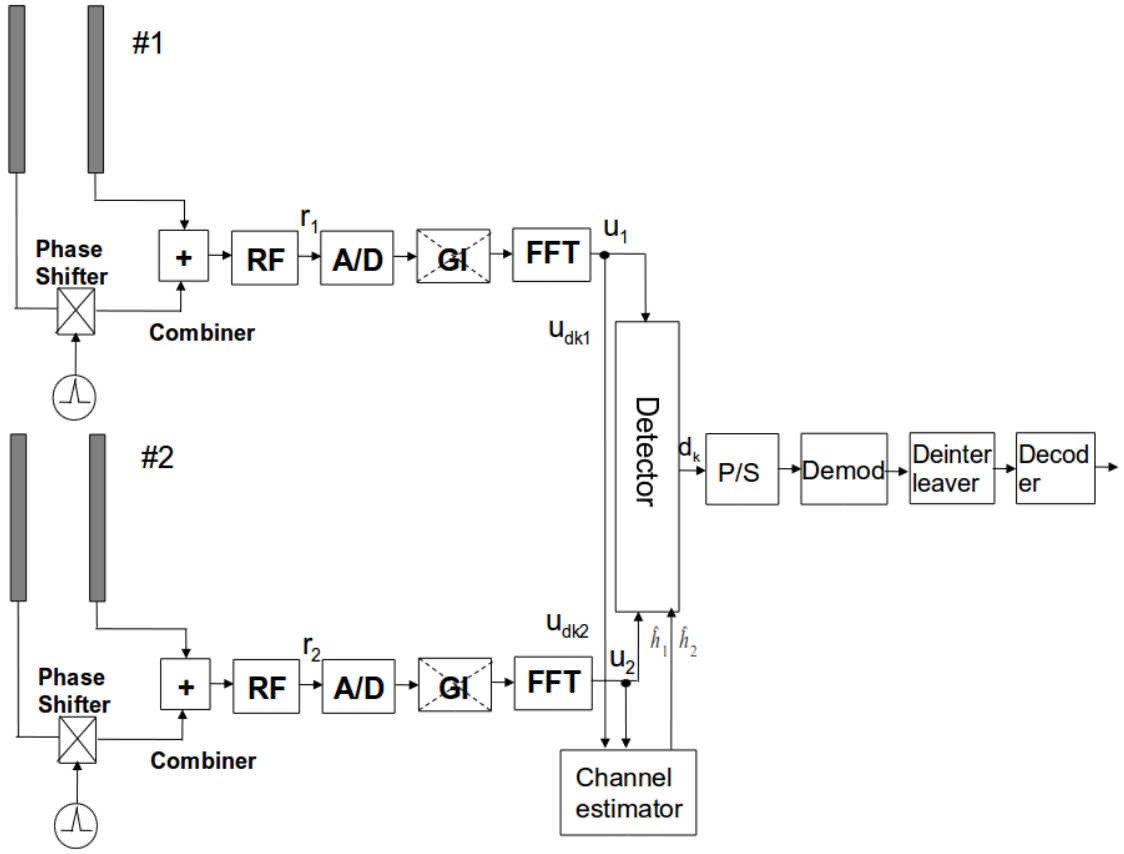

Figure 7.13. Block diagram of coded MIMO-OFDM RF signal-processing receiver

Table 7.1. Complexity of computational cost

MIMO detection	Multiplication	Addition
RF V-BLAST[13]	23.5 x 10^6	23.4 x 10^6
RF MMSE	11.86 x 10^6	11.7 x 10^6
Traditional MLD[13]	23.8 x 10^3	20 x 10^3
RF Kalman filter	**28.3** x $\mathbf{10^3}$	**28.2** x $\mathbf{10^3}$

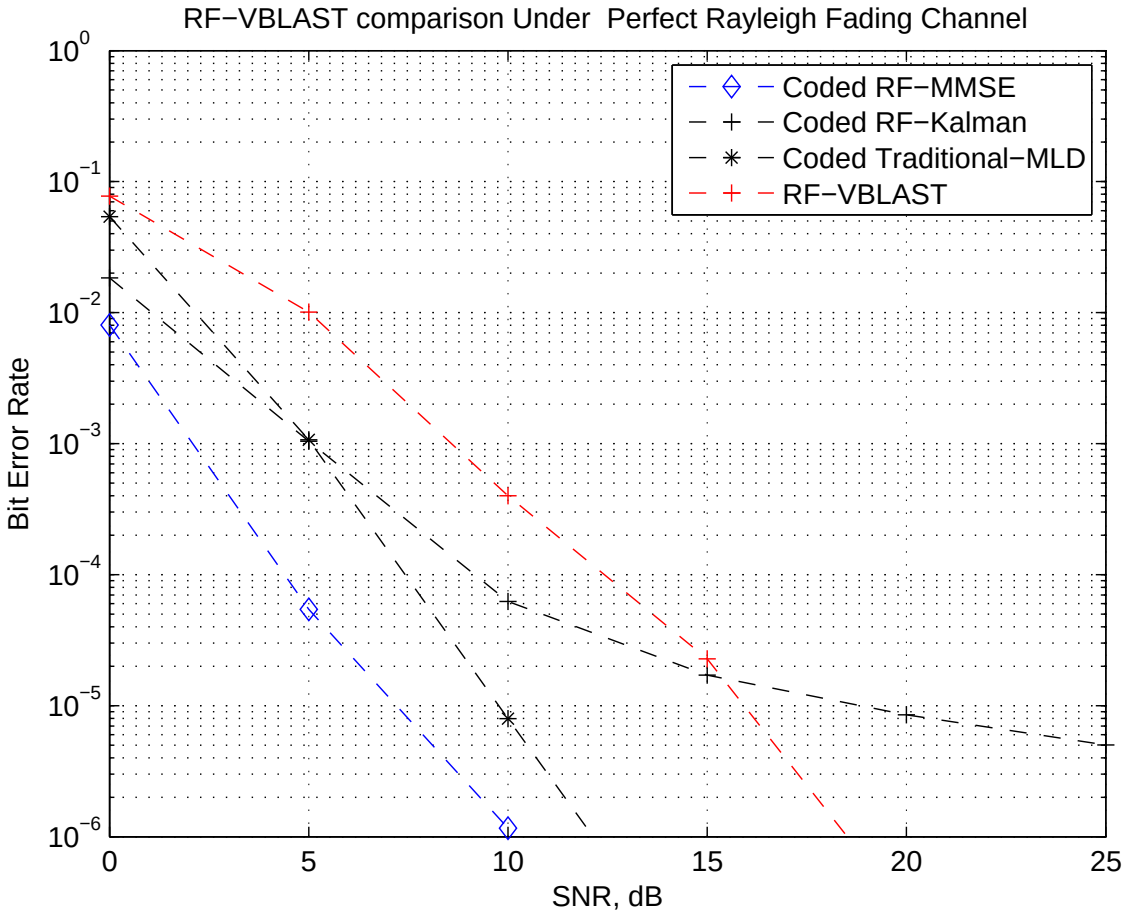

Figure 7.14. BER performance of RF-VBLAST comparison over perfect Rayleigh fading channel

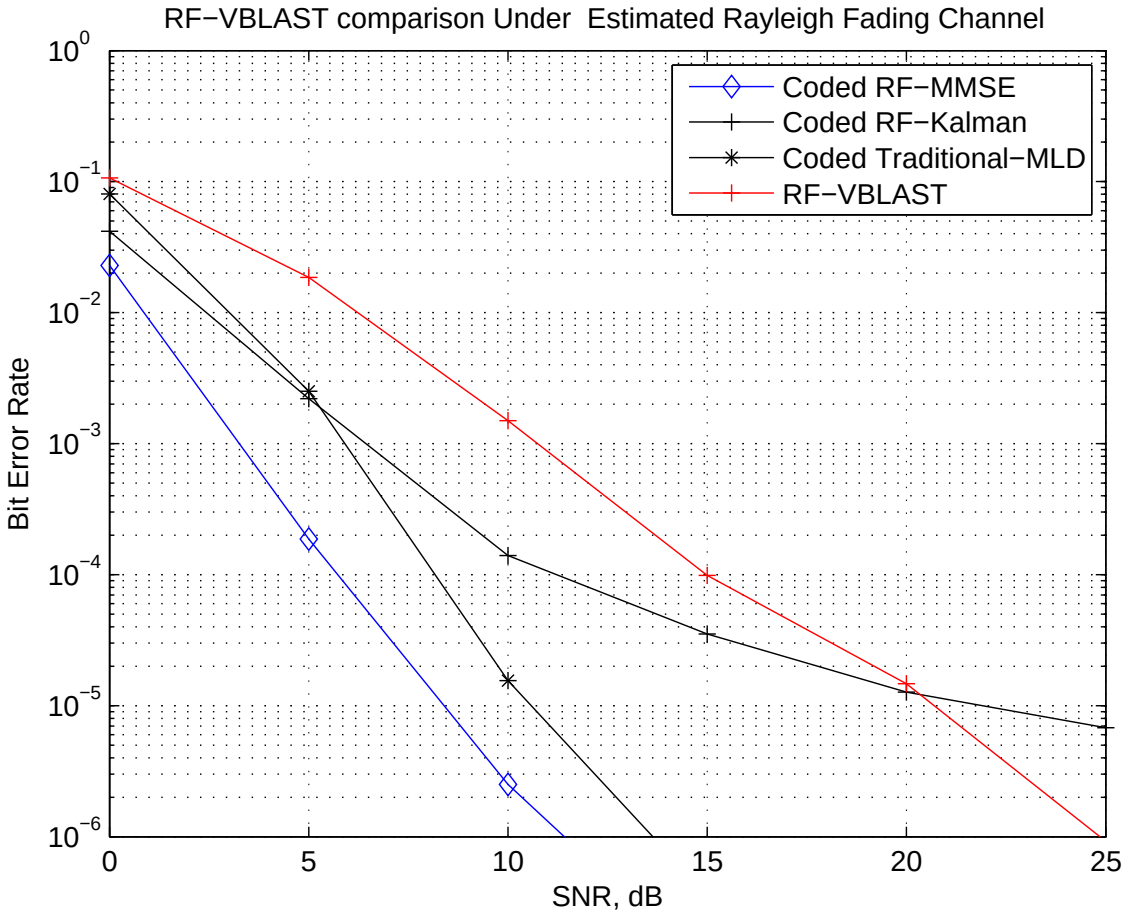

Figure 7.15. BER performance of RF-VBLAST comparison over estimated Rayleigh fading channel

Chapter 8

Conclusion

IN this dissertation, RF signal processing assisted MIMO-OFDM receiver has been proposed. Computer simulations has been carried out in order to confirm the validity of the proposed scheme. The results showed that the proposed receiver was capable of improving the bit error rate performance in a frequency selective fading enviroment without increasing in the hardware size. In a two-ray Rayleigh fading environment, the proposed scheme achieved the diversity gain of 10.9 dB in case of perfect channel estimation, and 9.45 dB when the MMSE-based channel estimator was employed. Although the proposed scheme is confirmed to be effective in terms of improving the bit error rate performance, the computational cost required for MIMO decomposition of the proposed MIMO-OFDM receiver is too huge to implement directly. Then, in order to reduce the computational cost, proposed the Kalman filter-based MIMO detector with ECC and it has successfully reduced the computational cost with relatively small degradation in the bit error rate performance.

Acknowledgements

This study was supported by Industrial Technology Research Grant program in 2009 from New Energy and Industrial technology Department Organization (NEDO) of Japan.

First of all and foremost, I thank to the God for His bless and merciful throughout all of my life. I also have many people to thank for helping to make my NAIST experience both enriching and rewarding.

First, I would like to express my profound gratitude to Professor Minoru Okada for the valuable ideas, discussion and research guidance. His encouragement has been the most valuable throughout my study at NAIST.

I would like to thank Professor Hiroyuki Seki and Professor Kenji Sugimoto for excellent technical discussion throughout all of my academic activities at NAIST as co-supervisors.

I would like to thank Professor Takao Hara for fruitful discussion by reading of the manuscript and excellent technical revision of the documents.

I would like to thank DIKTI, for giving me a chance to pursue my doctoral degree in Japan and valuable help and support during my stay in Japan.

Finally, I'll give my acknowledgements to all my Japanese friends or abroad, my present and past members of Communications Laboratory, who helped creating a very enjoyable and productive environment in the laboratory.

Through it all, I owe my greatest debt to my family, my parents, my wife and children. Your love, patient and support are the most rewarding experience of my graduate years.

References

[1] A.C. K.Vishnu Vardhan, Saif K Mohammed and B.S. Rajan, "A low-complexity detector for large mimo system and multicarrier *CDMA* system," IEEE Journal on Selected Areas in Communications, vol.26, no.3, pp.473–485, apr 2008.

[2] A. Goldsmith, Wireless Communications, Cambridge University Press, 2005.

[3] R.N. Arogyaswami Paulraj and D. Gore, Introduction to Space-Time Wireless Communications, Cambridge University Press, 2003.

[4] B. L.Hanzo, M.Munster and T.Keller, OFDM and MC-CDMA for Broadband Multi-User Communications, WLANs and Broadcasting, IEEE Press, 2003.

[5] A. Kalis, A.G. Kanatas, and C.B. Papadias, "A novel approach to MIMO transmission using a single RF front end," IEEE Journal on Selected Areas in Communications, vol.26, no.6, pp.972–980, Aug. 2008.

[6] S. Tsukamoto and M. Okada, "Single-RF maximal ratio combining diversity for OFDM system using an ESPAR antenna whose direction is oscillated in the symbol time," 2009 Thailand - Japan MicroWave, pp.1–4, June 2009.

[7] P.W. Wolniansky, G.J. Foschini, G.D. Golden, and R.A. Valenzuela, "V-blast: An architecture for realizing very high data rates over the rich-scattering wireless channel," Proceedings IEEE ISSSE-98.

[8] S.A.K.T. Imran Khan and N. Rajatheva, "Capacity and performance analysis of space-time block coded mimo-ofdm systems over rician fading channel," International Journal of Electrical and Computer Engineering, pp.974–980, 2009.

[9] L. Haring and A. Czylwik, "Synchronization in MIMO OFDM system," Advances in Radio Science, vol.2, no.1, pp.147–153, Jan. 2004.

[10] B. Shishkov and T. Ohira, "Adaptive beamforming of ESPAR antenna based on stochastic approximation theory," IEICE Technical Report, vol.40, no.47, pp.41–48, July 2001.

[11] T.W.G. of the 802 Committee, Draft Standard for Information Technology Telecommunication and Information Exchange between System Local and Metropolitan Area Networks Specific Requirements, Three Park Avenue, New York, 2007.

[12] G. Golden, C. Foschini, R. Valenzuela, and P. Wolniansky, "Detection algorithm and initial laboratory results using v-blast space-time communication architecture," Electronics Letters, vol.35, no.1, pp.14–16, Jan. 1999.

[13] I.G.P. Astawa and M. Okada, "ESPAR antenna-based diversity scheme for MIMO-OFDM systems," 2010 Thailand - Japan MicroWave, pp.1–4, Feb. 2010.

[14] A. Hiwale and A. Ghatol, "Performance of space- time block coded mimo systems with antenna selection," Proceedings of SPIT-IEEE Colloquium and International Conference Sardar Patel Institute of Technology, Andheri(w) Mumbai IEEE - BOMBAY SECTION, vol.3, no.134, Feb. 2008.

[15] X. Zhu and R.D. Murch, "Performance analysis of maximum likelihood detection in a mimo antenna system," IEEE Trans. Commun., vol.50, pp.187–191, Feb. 2002.

[16] B. Ristic and S. Arulampalam, Beyond the Kalman Filter: Particle Filters for Tracking Applications, Artech House, 2004.

[17] G.B. Greg Welch, "An introduction to the Kalman filter," Lecture Note, Department of Computer Science University of North Carolina at Chapel Hill, July, 2006.